AMERICAN SOCIETY FOR MICROBIOLOGY | Journal of Virology®

VACCINES AND ANTIVIRAL AGENTS

# Viral Subpopulation Screening Guides in Designing a High Interferon-Inducing Live Attenuated Influenza Vaccine by Targeting Rare Mutations in NS1 and PB2 Proteins

Amir Ghorbani,[a,b] Michael C. Abundo,[a] Hana Ji,[a,b] Kara J. M. Taylor,[a*] John M. Ngunjiri,[a] Chang-Won Lee[a,b]

[a]Food Animal Health Research Program, Ohio Agricultural Research and Development Center, The Ohio State University, Wooster, Ohio, USA
[b]Department of Veterinary Preventive Medicine, College of Veterinary Medicine, The Ohio State University, Columbus, Ohio, USA

**ABSTRACT** Influenza A viruses continue to circulate among wild birds and poultry worldwide, posing constant pandemic threats to humans. Effective control of emerging influenza viruses requires new broadly protective vaccines. Live attenuated influenza vaccines with truncations in nonstructural protein 1 (NS1) have shown broad protective efficacies in birds and mammals, which correlate with the ability to induce elevated interferon responses in the vaccinated hosts. Given the extreme diversity of influenza virus populations, we asked if we could improve an NS1-truncated live attenuated influenza vaccine developed for poultry (PC4) by selecting viral subpopulations with enhanced interferon-inducing capacities. Here, we deconstructed a *de novo* population of PC4 through plaque isolation, created a large library of clones, and assessed their interferon-inducing phenotypes. While most of the clones displayed the parental interferon-inducing phenotype in cell culture, few clones showed enhanced interferon-inducing phenotypes in cell culture and chickens. The enhanced interferon-inducing phenotypes were linked to either a deletion in NS1 (NS1Δ76-86) or a substitution in polymerase basic 2 protein (PB2-D309N). The NS1Δ76-86 deletion disrupted the putative eukaryotic translation initiation factor 4GI-binding domain and promoted the synthesis of biologically active interferons. The PB2-D309N substitution enhanced the early transcription of interferon mRNA, revealing a novel role for the 309D residue in suppression of interferon responses. We combined these mutations to engineer a novel vaccine candidate that induced additive amounts of interferons and stimulated protective immunity in chickens. Therefore, viral subpopulation screening approaches can guide the design of live vaccines with strong immunostimulatory properties.

**IMPORTANCE** Effectiveness of NS1-truncated live attenuated influenza vaccines relies heavily on their ability to induce elevated interferon responses in vaccinated hosts. Influenza viruses contain diverse particle subpopulations with distinct phenotypes. We show that live influenza vaccines can contain underappreciated subpopulations with enhanced interferon-inducing phenotypes. The genomic traits of such virus subpopulations can be used to further improve the efficacy of the current live vaccines.

**KEYWORDS** influenza, subpopulations, interferon, live attenuated vaccine, NS1, PB2

Influenza A viruses (IAVs) belong to the family *Orthomyxoviridae*. Their genomes consist of eight segments of negative-sense RNA in the form of ribonucleoprotein (RNP) complexes. Each RNP is associated with a heterotrimeric RNA-dependent RNA-polymerase complex and, therefore, can be transcribed immediately upon translocation to the nucleus of the infected cell (1). Owing to the lack of proofreading capability of the viral RNA polymerase complex, IAVs are prone to high rates of spontaneous

**Citation** Ghorbani A, Abundo MC, Ji H, Taylor KJM, Ngunjiri JM, Lee C-W. 2021. Viral subpopulation screening guides in designing a high interferon-inducing live attenuated influenza vaccine by targeting rare mutations in NS1 and PB2 proteins. J Virol 95:e01722-20. https://doi.org/10.1128/JVI.01722-20.

**Editor** Stacey Schultz-Cherry, St. Jude Children's Research Hospital



Address correspondence to John M. Ngunjiri, ngunjiri.1@osu.edu, or Chang-Won Lee, lee.2854@osu.edu.

* Present address: Kara J. M. Taylor, Department of Biology, University of Florida, Gainesville, Florida, USA.

**Received** 29 August 2020
**Accepted** 20 October 2020
**Accepted manuscript posted online** 28 October 2020
**Published** 22 December 2020

mutations, leading to extensive genomic and phenotypic diversity in the virus population (reviewed in references 2–4).

Seasonal IAV epidemics are a major cause of respiratory illness and mortality in humans. Global human pandemics can also arise through zoonotic transmission of emerging IAVs from animals (5). Migratory wild birds serve as natural reservoirs for all IAV subtypes (6, 7). Periodic introduction of IAVs, especially of the H5 and H7 subtypes, from wild birds to domestic poultry can have devastating effects on the poultry industry and global food security (8, 9). Although commercial vaccines have been shown to provide good protection against closely related IAVs, there is currently no effective and practical vaccine to control antigenic variants or newly emerging IAVs in poultry (10). Therefore, there is a growing need to develop novel universal vaccines that can effectively immunize the host against a wider range of IAV strains (11).

An ideal vaccine should efficiently activate both the innate and adaptive arms of immunity, similar to activation by natural IAV infection. The innate immune system, especially through interferons (IFNs), serves as one of the first layers of host defense against viral pathogens including IAVs (12). The activation of innate immunity also promotes the development of adaptive immune responses through mediator cytokines secreted from dendritic cells (12–14). Upon virus infection, activation of cellular pattern recognition receptors triggers a signaling cascade that leads to production of type I ($\alpha$ and $\beta$) and type III ($\lambda$) IFNs that, in turn, induce the expression of hundreds of IFN-stimulated genes with potent antiviral activities (12). To overcome this barrier and remain fully infectious, IAVs have evolved countermeasures to prevent or circumvent the activation of IFN response in infected cells. One of these countermeasures is the nonstructural protein 1 (NS1), a multifunctional viral protein that plays a central role in antagonizing the IFN system (reviewed in reference 15). Accordingly, IAVs expressing truncated NS1 proteins are highly attenuated while exhibiting an enhanced IFN-inducing phenotype in immunocompetent hosts, making them ideal candidates for development of effective live attenuated influenza vaccines (LAIVs) (reviewed in reference 16).

NS1-truncated LAIVs provide a robust protective immunity against diverse influenza virus strains in various hosts, including murine (17, 18), swine (19–21), equine (22, 23), avian (24–27), nonhuman primate (28), and human hosts (29). In our search for potential LAIV candidates, we found that A/turkey/OR/71-delNS1 (H7N3) virus contains multiple genetically and phenotypically diverse subpopulations of NS1-truncated variants (24, 30). Despite having similar levels of NS1 truncations, these variants displayed varying degrees of protective efficacies in avian (24, 30) and mammalian (31) species, which correlated with their ability to induce a type I IFN response in cells from the specific hosts (30–32). One of the naturally derived variants, the plaque clone 4 virus (PC4), was predicted to be highly protective in avian hosts based on its type I IFN-inducing ability in avian cells (30). PC4 expresses a naturally truncated NS1 protein maintaining only the first 91 (out of 230) amino acids at the N terminus and an additional two nonconsensus amino acids at the C terminus (24). In chickens, PC4 induces high levels of innate immune responses, is highly attenuated, and does not transmit to unvaccinated contact birds, making it a safe alternative for inactivated vaccines (24–26). Most importantly, PC4 has demonstrated the ability to induce rapid, robust, and cross-reactive systemic and mucosal antibody responses that translate into significant protective immunities against antigenically distant heterologous and heterosubtypic low-pathogenicity IAVs in chickens (24, 26, 27).

In this study, we asked whether we could further improve the IFN-inducing ability of PC4 for avian hosts. Owing to the intrinsic propensity of IAVs to form heterogenous particle subpopulations (2), we hypothesized that PC4 is naturally composed of subpopulations with enhanced IFN-inducing phenotypes. To test this hypothesis, we analyzed a large library of plaque-purified PC4 subpopulations and found a few subpopulations with enhanced IFN-inducing capacities. We identified two key mutations in NS1 and polymerase basic 2 (PB2) proteins that were linked to the high IFN-inducing phenotypes. We then combined the two mutations to engineer a new

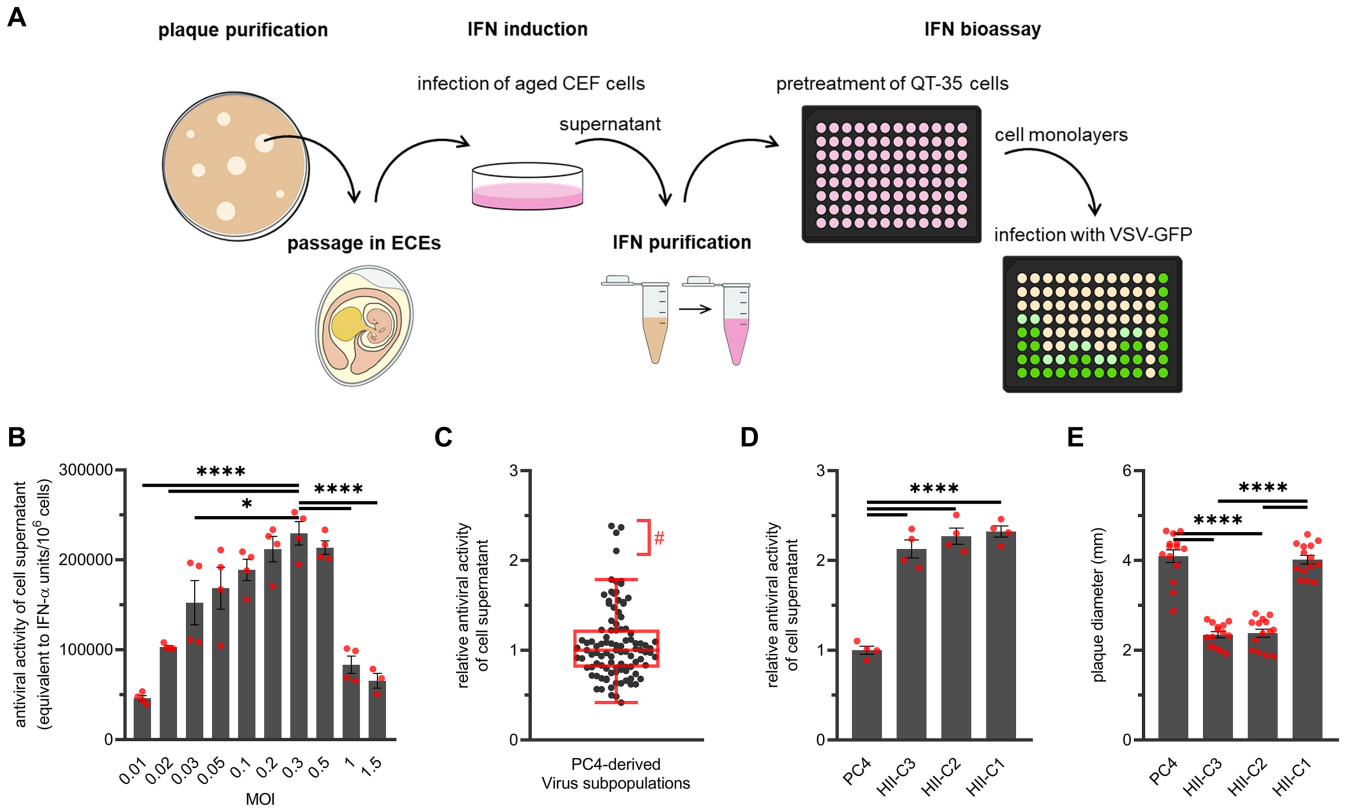


**FIG 1** IFN-based screening of PC4 virus subpopulation. (A) Schematic of the experimental approach. PC4 virus subpopulations were plaque purified in CEF cells and propagated in ECEs. Developmentally aged CEF cells were infected with each plaque-purified clone, and cell supernatants were collected at 24 hpi. The acid-stable type I IFN released into the cell supernatants was partially purified using perchloric acid treatment. To quantify the biological activity of the IFN, QT-35 cells were treated with serial 2-fold dilutions of the purified supernatants for 19 h and then challenged with a vesicular stomatitis virus that expresses GFP (VSV-GFP). At 24 hpi, GFP intensities were recorded, using a fluorescence plate reader, that were then used to extrapolate the concentration of IFN in the purified supernatants (IFN-$\alpha$ units/ml), using a recombinant chicken IFN-$\alpha$ as standard. (B) Induction of varying levels of type I IFNs by PC4 at different MOIs. IFN induction was performed by infecting the aged CEF cells with the indicated MOIs of PC4. IFN bioassay was performed as described above. Statistical differences were only shown for an MOI of 0.3 PFU/cell with the peak IFN yield, which was used for all future experiments. (C) Relative IFN-inducing profile of PC4 virus subpopulations. Experimental approach was as described above. The relative antiviral activity of cell supernatants was calculated by dividing the amounts of IFN induced by each virus by the average amounts induced by PC4 ($n = 4$) in the same assay. Black dots represent the average relative IFN-inducing capacity of each plaque-purified subpopulation obtained using three biological replicates. Graph includes pool data from multiple independent experiments. The overlaid Tukey's boxplot (red) displays the overall distribution of population and the presence of outliers (ROUT method of regression, Q coefficient = 5%; marked with #) with enhanced IFN induction (corresponded to HII-C1, HII-C2, HII-C3, and HII-C4). (D) Enhanced IFN induction by the HII-C1, HII-C2, and HII-C3 relative to the parental PC4. IFN induction (MOI = 0.3) and bioassay were performed as described above. (E) Formation of plaques with distinct diameters by the HII clones. Chicken embryo kidney cell monolayers were infected with the indicated clones (10 to 20 PFU/monolayer). At 80 hpi, the cell monolayers were fixed with 10% formalin and stained with 0.1% crystal violet to visualize the plaques. Plaque images were captured using the FluorChem Q imaging system (Alpha Innotech), and plaque diameters were measured using ImageJ software. Red dots represent values for each biological replicate. Bars indicate mean ± standard error of the mean (SEM) of biological replicates. ****, $P < 0.0001$; *, $P < 0.05$ (one-way ANOVA with Tukey's *post hoc* test).

LAIV candidate with exceptional IFN-inducing capacity in chickens. Our data showcase that subpopulation screening approaches can be used to improve the innate immunostimulatory property of LAIVs.

## RESULTS

**PC4 contains rare subpopulations with enhanced IFN-inducing phenotypes.** PC4, which was naturally derived from A/turkey/OR/71-delNS1 (H7N3) virus, was recreated *de novo* through reverse genetics (24). To investigate the diversity of IFN-inducing subpopulations of PC4, we isolated 100 clones from the population through plaque purification in chicken embryo fibroblast (CEF) cells and amplified each clone once in embryonated chicken eggs (ECEs). We then assessed the ability of the clones to induce type I IFNs in developmentally aged CEF cells as shown in Fig. 1A (33). To do that, we infected aged CEF cell monolayers with each clone at a multiplicity of infection (MOI) of 0.3 PFU per cell, which was determined to induce the peak IFN response by PC4 (Fig. 1B). We then collected the cell culture supernatants at 24 h postinfection (hpi),

**TABLE 1** Mutations identified in PC4 virus-derived plaque clones with enhanced or parental IFN-inducing capacities

| IFN-inducing phenotype | Plaque clone(s) | Protein | Mutation(s) |
|---|---|---|---|
| Enhanced | HII-C1 | PB2 | D309N |
| | HII-C2 and HII-C4 | NS1 | Deletion (position 76–86) |
| | | NA | F97L, E119A |
| | HII-C3 | NS1 | Deletion (position 76–86) |
| | | NA | F97L, E119A |
| | | HA | A168G |
| Parental | Clones 1 and 2 | None | None |
| | Clone 3 | NA | D127N |
| | Clone 4 | HA | I59V |
| | Clone 5 | HA | V332F |

precipitated acid-labile proteins from the supernatants, and analyzed the antiviral activity of acid-stable type I IFNs in the supernatants against vesicular stomatitis virus (VSV) infection in QT-35 cells (34–37). Finally, we compared the IFN-inducing capacities of the clones relative to PC4 (Fig. 1C). From the library of 100 plaque clones, 96 clones displayed IFN-inducing phenotypes that closely resembled that of the parental PC4. The remaining 4 clones were identified as population outliers with substantially enhanced IFN-inducing capacities compared to that of the population consensus by the ROUT method of regression (38). We then performed an independent experiment to confirm the enhanced IFN responses induced by the top 3 high IFN-inducing (HII) clones, hereafter referred to as clones HII-C1, HII-C2, and HII-C3 (Fig. 1D). HII-C4 was dropped from further phenotypic analysis because it was genetically identical to HII-C2 at the level of consensus sequences (Table 1). Interestingly, there was no direct relationship between plaque size and IFN-inducing phenotypes of the clones (Fig. 1 E). These results show that even highly purified *de novo* created viruses can contain rare subpopulations with HII phenotypes.

**The HII clones induce enhanced innate immune responses while maintaining their parental protective efficacies in vaccinated chickens.** To validate the IFN-inducing phenotypes *in vivo*, we inoculated separate groups of 2-week-old chickens with each of the three selected HII clones or PC4 via the intrachoanal and intraocular routes. Another group of chickens was subcutaneously inoculated with oil-adjuvanted inactivated PC4 vaccine (IIV), while the mock group was left untreated. We then euthanized a set of birds at 24 hpi ($n = 4$/group) to collect tracheas for transcriptional analysis of IFN and IFN-related genes. As illustrated in Fig. 2, the expression of IFN-$\beta$ (type I IFN) gene was significantly upregulated by all three HII clones, while that of IFN-$\gamma$ and IFN-$\lambda_3$ (type II and III IFNs, respectively) was upregulated only by HII-C1 compared to that of the mock group. The elevated IFN-$\beta$ gene expression corresponded with significant upregulation of downstream IFN-stimulated antiviral genes as follows: the myxovirus resistance protein 1 (MX1) and 2′-5′-oligoadenylate synthetase-like (OASL) genes (Fig. 2D and E). All three HII clones also stimulated a significant increase in expression of the mitochondrial antiviral signaling protein (MAVS) gene compared to the mock and IIV groups (Fig. 2F). Overall, these results verified the enhanced IFN-inducing ability of the HII clones *in vivo*. The results highlight the predictive accuracy of our cell culture-based approach for selecting mutants with higher innate immunostimulatory capacities in their target hosts (30).

We tracked the other set of birds ($n = 7$/group) to determine the progression of humoral (serum) and mucosal (tear) antibody responses up to 3 weeks postvaccination (WPV). Homologous hemagglutination inhibition (HI) antibodies were detected in serum samples derived from vaccinated chickens at 1 WPV and continued to increase for the duration of the experiment (Fig. 3A). As previously observed with PC4 vaccination (26), higher seroconversion rates were observed in all live vaccine groups (PC4 and HII clones) at 1 WPV compared to the IIV group. However, the HI titers of the IIV group thereafter increased by severalfold and were significantly higher than all live vaccine groups at 2 and 3 WPV. There were no significant differences in HI antibody titers

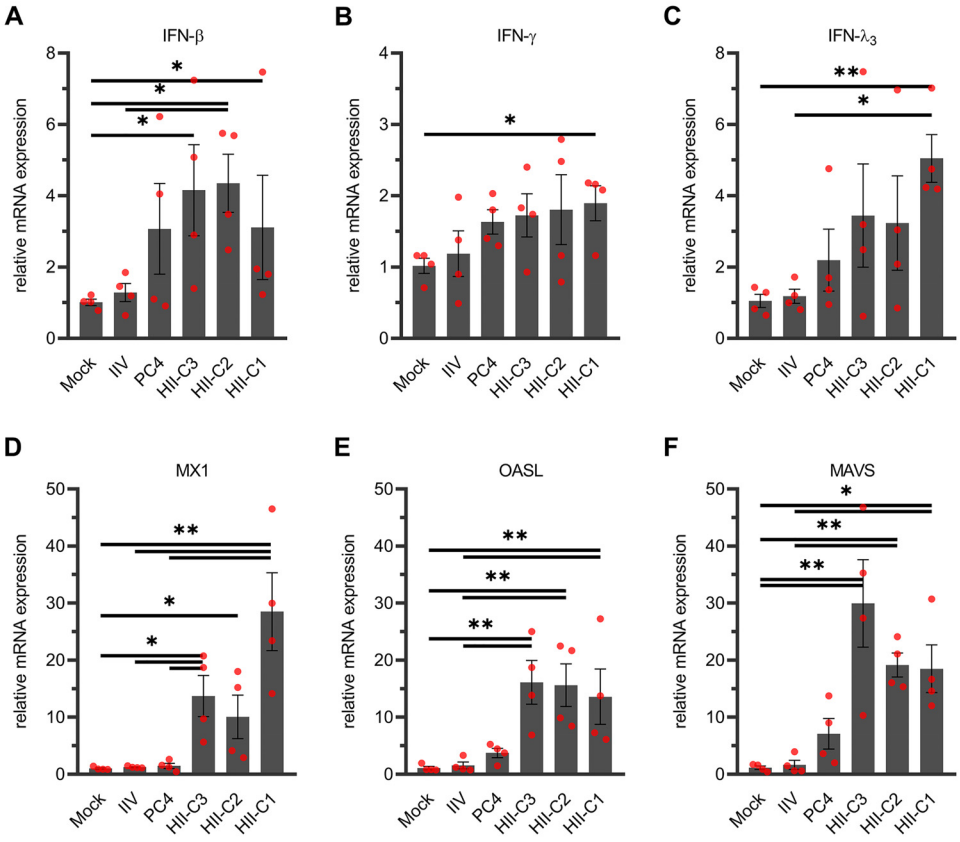


**FIG 2** Expression of IFN and IFN-related genes in vaccinated chickens. Two-week-old chickens were either vaccinated with the HII clones (HII-C1, HII-C2, and HII-C3) or PC4 ($10^6$ $EID_{50}$) via the intrachoanal and intraocular routes (1:1 ratio, vol/vol), injected subcutaneously with oil-adjuvanted inactivated PC4 vaccine (IIV), or left unvaccinated (mock). At 24 h postvaccination, chicken tracheas ($n = 4$/group) were collected, and the relative mRNA expression of IFN-$\beta$ (A), IFN-$\gamma$ (B), IFN-$\lambda_3$ (C), MX1 (D), OASL (E), and MAVS (F) genes in the tracheal tissue were determined using quantitative RT-PCR. Dots represent values for individual chickens. Bars indicate mean ± SEM of chicken groups. **, $P < 0.01$; *, $P < 0.05$ (Kruskal-Wallis test).

among the live vaccine groups except at 3 WPV when the HII-C1 group showed significantly higher titers than the HII-C3 group. Similar trends were observed when a heterologous H7N2 low-pathogenicity avian influenza virus (A/chicken/NJ/150383-7/02) antigen was used against the 3 WPV prechallenge serum samples in the HI assay (Fig. 3B). Influenza virus-specific IgA antibody titers in chicken tears were in great accordance with the serum HI titers among live virus immunization groups. However, the IIV group did not develop detectable IgA titers (Fig. 3C) despite having the highest serum HI antibody titers among the groups (Fig. 3A and B). Significantly higher levels of tear IgA were observed in both HII-C1 and PC4 groups compared to those of the mock, IIV, and HII-C3 groups. Collectively, these data show that the humoral (serum) and mucosal (tear) antibody-inducing phenotypes of the HII clones generally follow the same trend as the live parental PC4.

At 3 WPV, we examined the protective efficacy of the vaccines by challenging the chickens ($n = 7$/group) with the heterologous H7N2 virus and determined the levels of challenge virus shedding in tracheas. Regardless of the lower humoral and mucosal antibody titers observed in some groups (especially HII-C2 and HII-C3), all of the vaccinated groups showed significant reduction in tracheal virus shedding during the peak of virus replication at 5 days postchallenge (DPC) compared to that of the mock group (Fig. 3D). In accordance with the overall higher levels of serum and mucosal antibody titers than the other live vaccine groups, the HII-C1 group also showed significant reduction in virus shedding compared to that of the mock group at 3 DPC. However, the differences in virus shedding titers between the vaccinated groups were

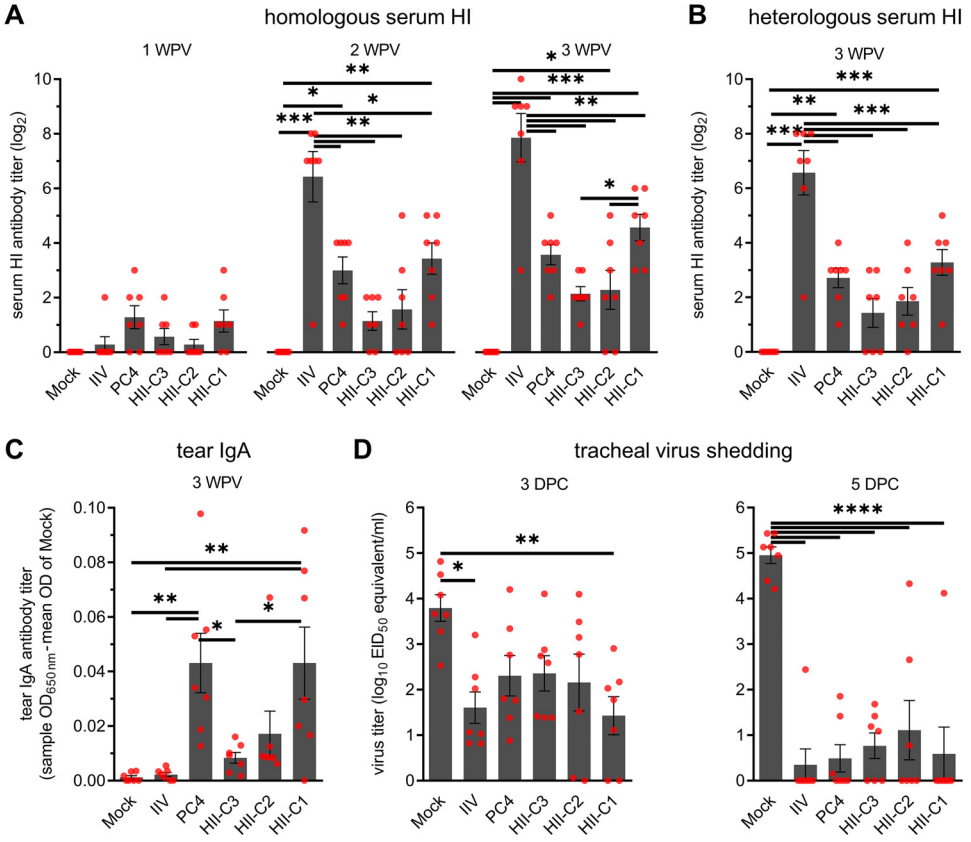


**FIG 3** Induction of humoral (A and B) and mucosal (C) antibodies and protective immunity (D) in vaccinated chickens. Two-week-old chickens were vaccinated as described in Fig. 2. (A) Homologous HI antibody titers in serum samples of vaccinated chickens at 1, 2, and 3 WPV. (B) Heterologous HI antibody titers against the challenge virus antigen in serum samples of vaccinated chickens at 3 WPV (1 day prior to challenge). (C) Influenza virus-specific IgA antibody titers in chicken tears at 3 WPV, as determined by a commercial IDEXX ELISA kit. IgA titers are shown as sample optical density at 650 nm ($OD_{650}$) minus the mean OD of mock. (D) Protective efficacies against the heterologous H7N2 challenge virus. At 3 WPV, chickens were challenged with an antigenically distant H7N2 virus ($10^6$ $EID_{50}$/bird), and the tracheal shedding of the virus was determined using quantitative RT-PCR at 3 and 5 DPC. Viral titers are expressed as $\log_{10}$ $EID_{50}$ equivalent per milliliter of the tracheal swab elutes (1 ml/swab). Dots represent values for individual chickens. Bars indicate mean ± SEM of chicken groups. ****, $P < 0.0001$; ***, $P < 0.001$; **, $P < 0.01$; *, $P < 0.05$ (one-way ANOVA with Tukey's *post hoc* test).

statistically indistinguishable. Overall, the protective efficacies of the HII clones and PC4 were similar under the experimental conditions used in this experiment.

**HII phenotypes are determined by a deletion in NS1 or a substitution in PB2.** To establish the genetic basis of enhanced IFN induction, we deep sequenced plaque clones with high ($n = 4$) and parental ($n = 5$) IFN-inducing phenotypes along with PC4. Table 1 presents the mutations found in the consensus genomes of sequenced plaque clones in comparison with PC4. Plaque clones with the parental IFN-inducing phenotype were either identical to PC4 or possessed single amino acid substitutions in hemagglutinin (HA) or neuraminidase (NA) proteins (Table 1). Accordingly, the consensus genomes of all of the 96 clones displaying the parental phenotype are likely to be highly similar. Apart from a few mutations observed in HA and/or NA proteins, 3 of the HII clones (HII-C2, HII-C3, and HII-C4) had a deletion of 11 amino acids at positions 76 to 86 (NS1Δ76-86) within the flexible linker region of the NS1 protein (amino acids 73 to 85) (Fig. 4A) (39). The NS1Δ76-86 deletion is unlikely to be an artifact of the plaque purification process because it was present at an average frequency of ~3% in two sequencing replicates of the parental PC4. The remaining HII clone (HII-C1) had a substitution of asparagine (N) for aspartic acid (D) at position 309 of the PB2 protein (PB2-D309N), which is located within the PB2 midlink domain (residues 251 to 315 [mid] and 490 to 536 [link]) and in proximity to the cap-binding domain of the viral

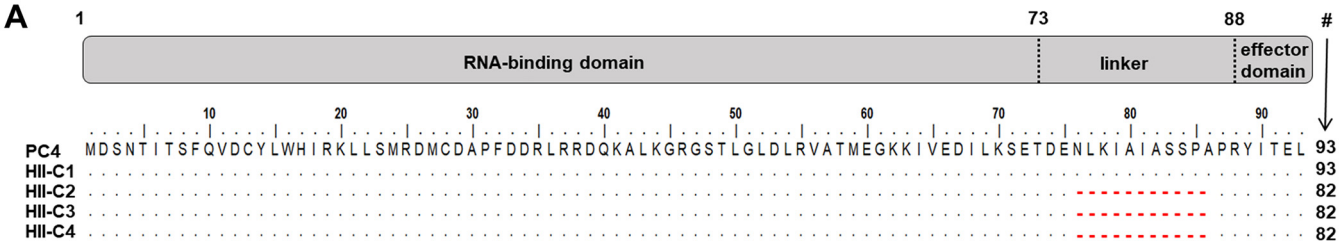


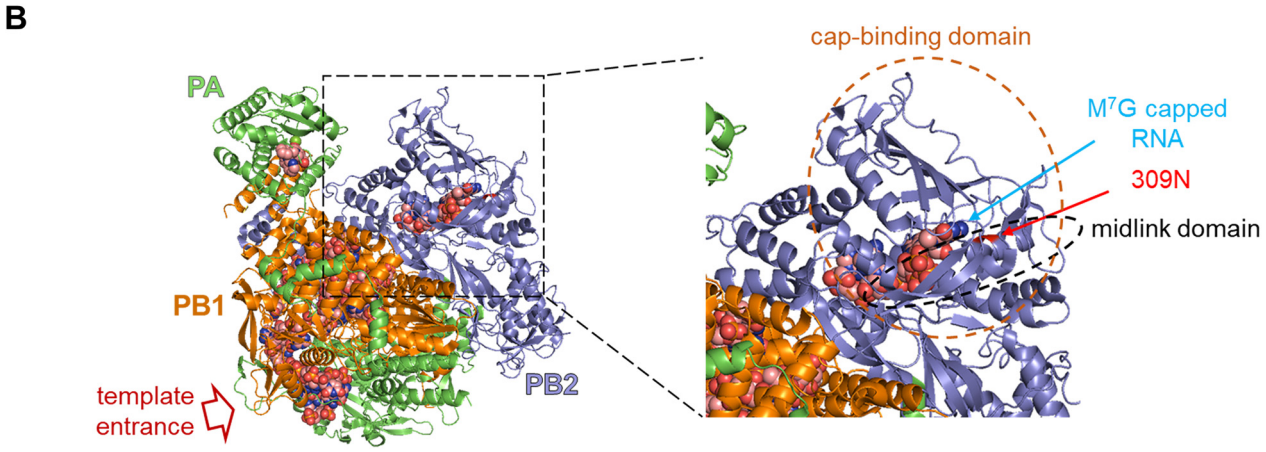


C

| | number of strains containing indicated amino acids at position 309 of PB2 protein | | | | | | | | | |
|---|---|---|---|---|---|---|---|---|---|---|
| subtype | D | N | E | G | S | H | Y | C | V | number of strains |
| H5 | 2235 | 28 | 23 | 30 | 0 | 2 | 0 | 0 | 0 | 2318 |
| H7 | 1103 | 9 | 4 | 4 | 3 | 0 | 0 | 0 | 0 | 1123 |
| H9 | 1430 | 10 | 1 | 10 | 0 | 0 | 1 | 0 | 0 | 1452 |
| all others | 5548 | 26 | 43 | 20 | 0 | 0 | 1 | 1 | 1 | 5640 |
| total (all subtypes) | 10316 | 73 | 71 | 64 | 3 | 2 | 2 | 1 | 1 | 10533 |
| occurrence (% of total # of strains) | 97.94 | 0.69 | 0.67 | 0.61 | 0.03 | 0.02 | 0.02 | 0.01 | 0.01 | |

**FIG 4** Sequence and structural analysis of the NS1 (Δ76-86) and PB2 (D309N) mutations found in the HII clones (HII-C1, HII-C2, HII-C3, and HII-C4). (A) Deletion of amino acids 76 to 86 severely disrupts the linker region of NS1 protein. NS1 proteins were aligned using the ClustalW algorithm in BioEdit (version 7.2.5). The gray box at the top indicates the RNA-binding and effector domains (residues 1 to 73 and 88 to #, respectively) of the NS1 protein, separated by a short linker region. Red dashed lines indicate the deletion of residues 76 to 86 of indicated viruses. For comparison, the wild-type NS1 protein of the A/turkey/OR/71 strain is 230 amino acids long. (B) The mutated amino acid 309 of PB2 protein (309N) is located within the PB2 midlink domain and in proximity to the cap-binding domain of the viral polymerase complex. PB2-309N residue was mapped onto the crystal structure of IAV polymerase complex (PDB accession number 6T0V) in PyMOL molecular graphics system (version 2.3.2). The space-filling molecule (marked with $m^7$G-capped RNA) represents the proximal part of the capped primer bound to the cap-binding domain in the early elongation stage. (C) PB2-309N amino acid is rarely found in avian influenza viruses in nature. The frequency of mutations at position 309 of PB2 protein of the previously isolated avian influenza viruses was determined based on the number of strains containing the mutation/total number of strains available in Influenza Research Database.

polymerase complex (Fig. 4B) (40, 41). We were unable to detect the PB2-D309N substitution in deep sequences obtained from the parental PC4, which is likely due to the low sequencing read depth at nucleotide 952 (an average of 584 reads), where the nonsynonymous mutation occurs. The PB2-D309N substitution was previously shown to increase the activity of viral polymerase complex, which can be beneficial to the virus (40). However, when we assessed the frequency of the PB2-D309N mutation in avian influenza viruses in the Influenza Research Database (42), we found it to be extremely rare, suggesting that this mutation may not be evolutionarily beneficial for the virus (Fig. 4C). Furthermore, none of the viruses in the database possessed the NS1Δ76-86 mutation. Of note, a smaller deletion at position 80 to 84 of the NS1 is commonly found in H5 avian influenza viruses (43). We also analyzed the deep sequences of the parental PC4 and plaque clones to determine the frequencies of minor single-nucleotide vari-

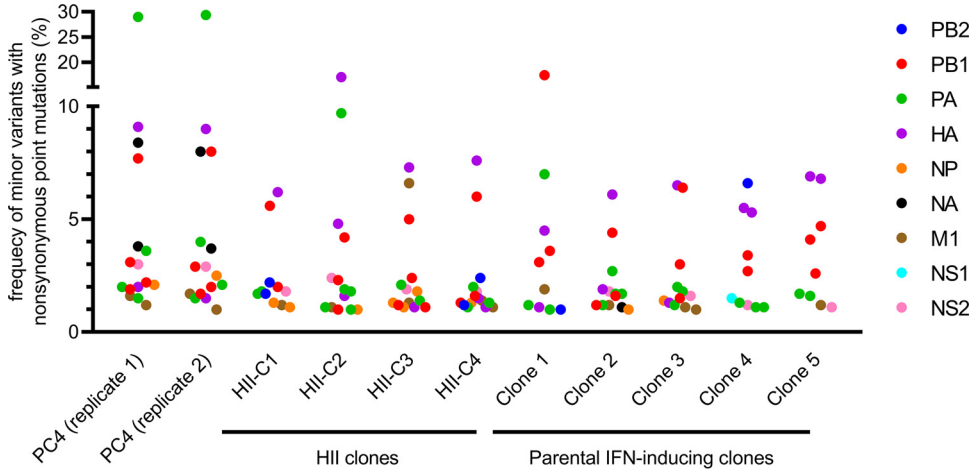


**FIG 5** Frequency of minor variants with nonsynonymous point mutations in the deep sequences of the parental PC4 and its plaque clones. Minor single-nucleotide variants with missense mutations were detected using the INSaFLU bioinformatics pipeline. Minor variants with synonymous mutations or nucleotide deletions/insertions are not shown in this graph. Dots represent the frequency of occurrence for individual minor variants. Different colors represent the viral protein in which the mutation occurred.

ants with nonsynonymous (missense) point mutations. The minor variants were generally detected at low frequencies (<10%) in virtually all genes, with no distinguishing patterns between the parental PC4 and plaque clones or between clones with HII and parental IFN-inducing phenotypes (Fig. 5). Overall, these results indicate that the rare NS1Δ76-86 and PB2-D309N mutations are responsible for the HII phenotypes of the respective plaque clones. Our finding also suggests a potential role for the 309D residue of the PB2 protein, which is present in >97% of avian influenza viruses, in suppression of IFN responses in avian hosts.

**NS1Δ76-86 and PB2-D309N mutations play nonredundant roles in induction of biologically active IFN.** To confirm the role of the newly discovered NS1 and PB2 mutations in IFN enhancement, we engineered them into reverse genetics plasmids for PC4 (24) and rescued new mutants with single (NS1Δ76-86 or PB2-D309N) or double (PB2-D309N/NS1Δ76-86) mutations (Fig. 6A). We then infected aged CEF cells with the newly generated mutants (MOI = 0.3) and quantified the antiviral activity of the acid-stable type I IFN released into the cell culture supernatants at 24 hpi. As shown in Fig. 6B, both PB2-D309N and NS1Δ76-86 mutants induced significantly higher levels of IFN compared to those of PC4, which reproduced the findings with the plaque clones possessing the PB2 (HII-C1) and NS1 (HII-C2, HII-C3, HII-C4) mutations, respectively (Fig. 1D). Strikingly, the PB2-D309N/NS1Δ76-86 double mutant induced significantly higher levels of IFN compared to those of the viruses with single mutations (Fig. 6B). The amount of IFN induced by the double mutant was roughly equal to the combined amount induced by both single mutants. The newly generated PB2-D309N and NS1Δ76-86 single mutants closely reproduced the plaque size profile differences observed between the plaque clones possessing the PB2 (HII-C1) and NS1 (HII-C2, HII-C3) mutations, respectively (Fig. 6C). Notably, the plaque diameters of the PB2-D309N/NS1Δ76-86 double mutant were significantly smaller than those of the single mutants or PC4. Altogether, these lines of evidence clearly demonstrate that the NS1Δ76-86 and PB2-D309N mutations play nonredundant roles in the enhancement of IFN response in infected avian cells and are directly linked to the plaque size phenotypes of the HII clones.

**NS1Δ76-86 and PB2-D309N mutations synergistically induce IFN-$\beta$ expression.** To confirm the effects of the NS1 and PB2 mutations on type I IFN response at the mRNA level, we infected QT-35 cell monolayers with the newly generated mutants (MOI = 0.3) and determined the expression of IFN-$\beta$ mRNA at 8 hpi. At this time point, significant expression of IFN-$\beta$ was evident in cells infected with PC4 or the newly

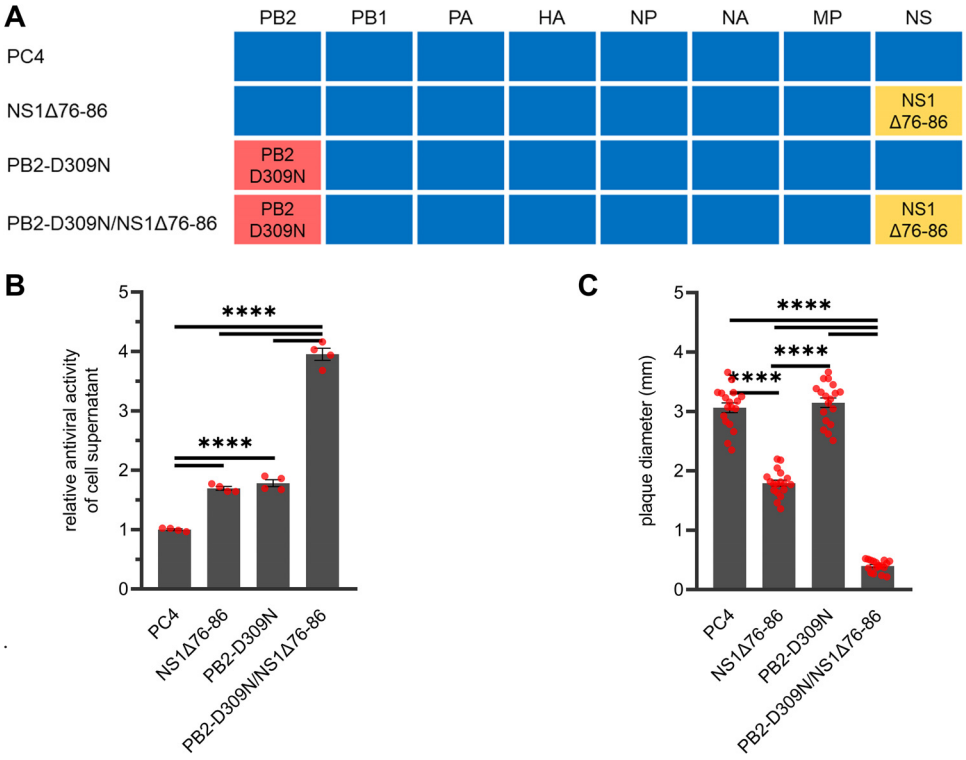


**FIG 6** *De novo* generation of recombinant viruses with enhanced IFN-inducing capacities in PC4 virus backbone. (A) Schematic diagram of the recombinant mutants generated in this study. The blue rectangles represent the genes of PC4, while yellow and red rectangles represent genes containing the NS1Δ76-86 and PB2-D309N mutations, respectively. (B) Enhanced IFN-inducing capacities of the newly engineered mutants in cell cultures relative to the parental PC4. IFN induction (MOI = 0.3) and bioassay were performed as described in Fig. 1A. (C) Formation of plaques with distinct diameters by the recombinant viruses with enhanced IFN-inducing phenotypes. Chicken embryo kidney cell monolayers were infected with the indicated viruses (10 to 20 PFU/monolayer). At 72 hpi, the cell monolayers were fixed, and the plaque diameters were determined as described in Fig. 1E. Dots represent values for individual biological replicates. Bars indicate mean ± SEM of biological replicates. ****, $P < 0.0001$ (one-way ANOVA with Tukey's *post hoc* test)

generated mutants compared to the mock (Fig. 7A). The mRNA levels generally confirmed the levels of biologically active type I IFNs induced in aged CEF cells, except for the NS1Δ76-86 mutant (Fig. 6B and 7A). Furthermore, there was a synergistic effect of the NS1 and PB2 mutations on IFN-$\beta$ mRNA upregulation since the level of expression in the double mutant was severalfold higher than the sum of expression values for the NS1Δ76-86 and PB2-D309N mutants (Fig. 7A).

**Amino acids 76 to 86 of NS1 are essential for the suppression of biologically active IFN synthesis.** Despite being able to induce significantly higher amounts of biologically active IFNs in aged CEF cells (Fig. 6B), the NS1Δ76-86 mutant induced similar levels of IFN-$\beta$ mRNA compared to those of PC4 in QT-35 cells at 8 hpi (Fig. 7A). We hypothesized that a substantial amount of the IFN-$\beta$ mRNAs induced by PC4 are not translated into biologically active IFN. To test this hypothesis, we focused on the QT-35 cells to eliminate any possible cell type- and host-specific differences in IFN response from our analysis. We infected QT-35 cell monolayers with the NS1Δ76-86 mutant and PC4 (MOI = 0.3) and examined the cells and supernatant medium for the levels of IFN-$\beta$ mRNA and biologically active IFN, respectively. For this experiment, we chose the 24-hpi time point because it represents the peak of biologically active IFN production in our single-cycle replication assay (35). As observed earlier in aged CEF cells (Fig. 6B), the levels of biologically active IFN induced by the NS1Δ76-86 mutant in QT-35 cells were significantly higher than those of PC4 (Fig. 7B). However, IFN-$\beta$ mRNA levels were statistically indistinguishable between the two tested viruses (Fig. 7C). These results indicate that the amino acid residues at positions 76 to 86 of the NS1 protein encoded

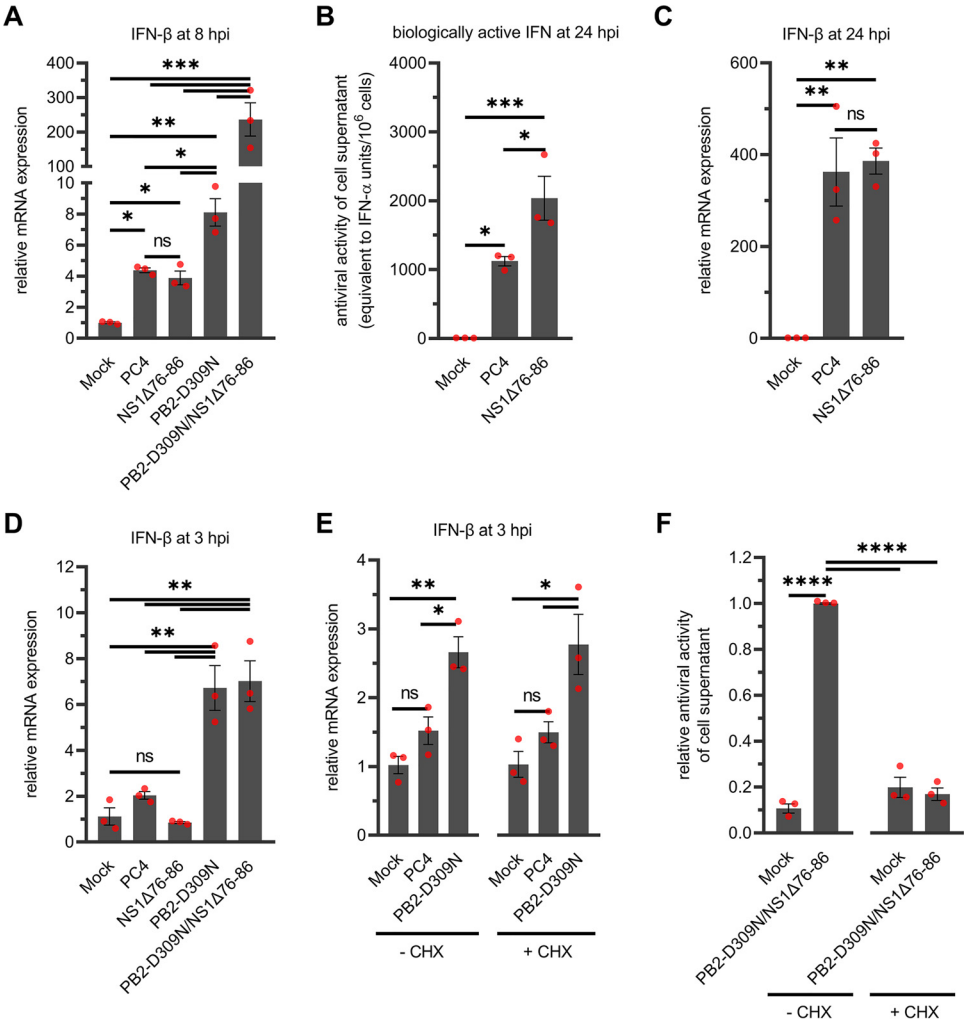


**FIG 7** Dynamics of type I IFN responses in infected cell monolayers. QT-35 cells were infected with the indicated viruses at an MOI of 0.3 and relative mRNA expression of IFN-$\beta$ gene in cell monolayers (A, C, D, E) or biological activity of acid-stable type I IFNs released into the cell supernatants (B, F) were determined at the indicated time points. IFN-$\beta$ mRNA levels were determined using quantitative RT-PCR. IFN induction and bioassay were performed in QT-35 cells following the protocol described in Fig. 1A. (A) synergistic effects of the NS1Δ76-86 and PB2-D309N mutations on IFN-$\beta$ mRNA expression at 8 hpi. Elevated levels of biologically active IFNs (B) but not IFN-$\beta$ mRNA (C) are induced by the NS1Δ76-86 mutant at 24 hpi. (D) Early induction of IFN-$\beta$ mRNA by the mutants encoding the PB2-D309N mutation at 3 hpi. (E) Elevated levels of IFN-$\beta$ mRNA expression are induced by the PB2-D309N mutant in cell monolayers treated with cycloheximide (+CHX) or left untreated (−CHX) at 3 hpi. (F) Cycloheximide-mediated block of protein synthesis was confirmed by the absence of functional IFN proteins in the supernatants of treated cells at 24 hpi. Relative antiviral activity of cell supernatants was calculated by dividing the IFN units induced in each sample by the average amounts induced by the virus in untreated cells. Dots represent values for each biological replicate. Bars indicate mean ± SEM of biological replicates. ****, $P < 0.0001$; **, $P < 0.01$; *, $P < 0.05$; ns, nonsignificant (one-way ANOVA with Tukey's *post hoc* test).

by PC4 constitute a domain that is required to suppress the translation of IFN mRNA into biologically active protein in avian cells.

**PB2-D309N mutation enhances the early induction of IFN mRNA synthesis.** Although the PB2-D309N mutation was previously shown to enhance viral polymerase activity in mammalian cells (40), its role in enhancement of IFN responses is not likely due to increased virus replication given the discordance between IFN responses and viral plaque diameters (Fig. 6B and C and Fig. 7A to C). For that reason, we hypothesized that the PB2-D309N mutation disables the ability of PB2 protein to suppress IFN mRNA transcription rather than increasing the number of IFN-inducing moieties (viral RNAs). To test that hypothesis, we infected QT-35 cells (MOI = 0.3) and assessed the expression of IFN-$\beta$ mRNA at 3 hpi, a time point at which new viral proteins are yet to be

produced (44, 45). Significant upregulation of IFN-$\beta$ mRNA was only evident in the cells infected with the single or double mutants with the PB2-D309N mutation compared to that of the mock-infected cells or those infected with the NS1Δ76-86 mutant or PC4 (Fig. 7D). To rule out the possibility that some new viral proteins might still be synthesized at this early time point, we treated virus-infected cells with cycloheximide, which inhibits translation elongation (46). Cycloheximide did not block the accumulation of IFN-$\beta$ mRNA in the cells infected with the PB2-D309N mutant (Fig. 7E), but it was able to prevent the synthesis of biologically active type I IFNs (Fig. 7F). Collectively, these results show that the PB2-D309N mutation destabilizes the early suppression of IFN mRNA synthesis, resulting in rapid IFN induction by the mutant virus.

**PB2-D309N/NS1Δ76-86 double mutant stimulates higher levels of innate immune responses in chickens.** To determine the immunogenicity of the newly engineered mutants in chickens, we vaccinated 2-week-old chickens with the PB2-D309N or NS1Δ76-86 single mutants, the PB2-D309N/NS1Δ76-86 double mutant, or PC4 as described earlier. Accordingly, the mock and IIV groups were also included in this experiment. The newly engineered mutants closely reproduced the innate immune responses induced by the HII clones in chicken tracheas at 24 hpi (Fig. 2 and 8). Compared to the mock group, there was induction of significant upregulation of IFN-$\beta$, OASL, and MAVS mRNA levels by single and double mutants, MX1 by the NS1Δ76-86 and double mutants, and IFN-$\lambda_3$ only by the double mutant (Fig. 8A and C to F). Neither PC4 nor IIV stimulated significant upregulation of any of the tested genes at 24 hpi (Fig. 8). Overall, the double mutant with a combination of the NS1Δ76-86 and PB2-D309N mutations proved to be superior to PC4 regarding innate immune stimulation in chickens.

Next, we evaluated the vaccine candidates for their ability to induce early humoral (serum) and mucosal (tear) antibody responses and protection in terms of reduction in tracheal virus shedding. At 6 DPV (1 day prior to challenge), several birds in the groups vaccinated with live virus (PB2-D309N/NS1Δ76-86, PB2-D309N, NS1Δ76-86, and PC4 groups) were positive for serum HI antibodies against the homologous virus antigen and tear IgA antibodies, but the overall antibody titers were statistically indistinguishable from those of the mock group (Fig. 9A and C). Interestingly, the PB2-D309N/NS1Δ76-86, PB2-D309N, and PC4 live vaccine groups started to show significant reduction in tracheal shedding of the heterologous H7N2 challenge virus as early as 3 DPC when compared to that of the mock group (Fig. 9D). Moreover, only the groups vaccinated with live vaccines shed significantly less virus at 5 DPC relative to the mock group (Fig. 9D) even in the absence of significant levels of humoral and mucosal antibodies (Fig. 9A to C). Among the vaccinated groups, the PB2-D309N/NS1Δ76-86 and PB2-D309N groups shed significantly less virus than the IIV group at 5 DPC (Fig. 9D), suggesting an improvement in early protective immunity provided by these new LAIV candidates compared to that of IIV. We continued to monitor the development of serum and tear antibodies in another subset of chickens ($n = 8$/group) up to 3 WPV. Among the groups vaccinated with live vaccines, serum HI antibody titers were significantly higher in the chickens vaccinated with PB2-D309N than those vaccinated with the NS1Δ76-86 and the double mutant at 2 and/or 3 WPV (Fig. 10A). Conversely, tear IgA antibody levels were significantly higher in the PB2-D309N and PC4 groups than in the mock and IIV groups (Fig. 10B). Collectively, these data highlight that combining the PB2-D309N and NS1Δ76-86 mutations can stimulate higher levels of innate immunity in the vaccinated chickens.

## DISCUSSION

NS1-truncated LAIVs can efficiently stimulate mucosal immunity that is instrumental in controlling IAV infection in vaccinated hosts. Like other IAVs, NS1-truncated LAIVs can contain genetically and phenotypically heterogeneous subpopulations. Here, we analyzed a large library of PC4-derived virus subpopulations and found them to greatly maintain their parental IFN-inducing phenotype, except for a few (4 out of 100) that exhibited the HII phenotypes (Fig. 1C). Similar HII phenotypes were previously reported

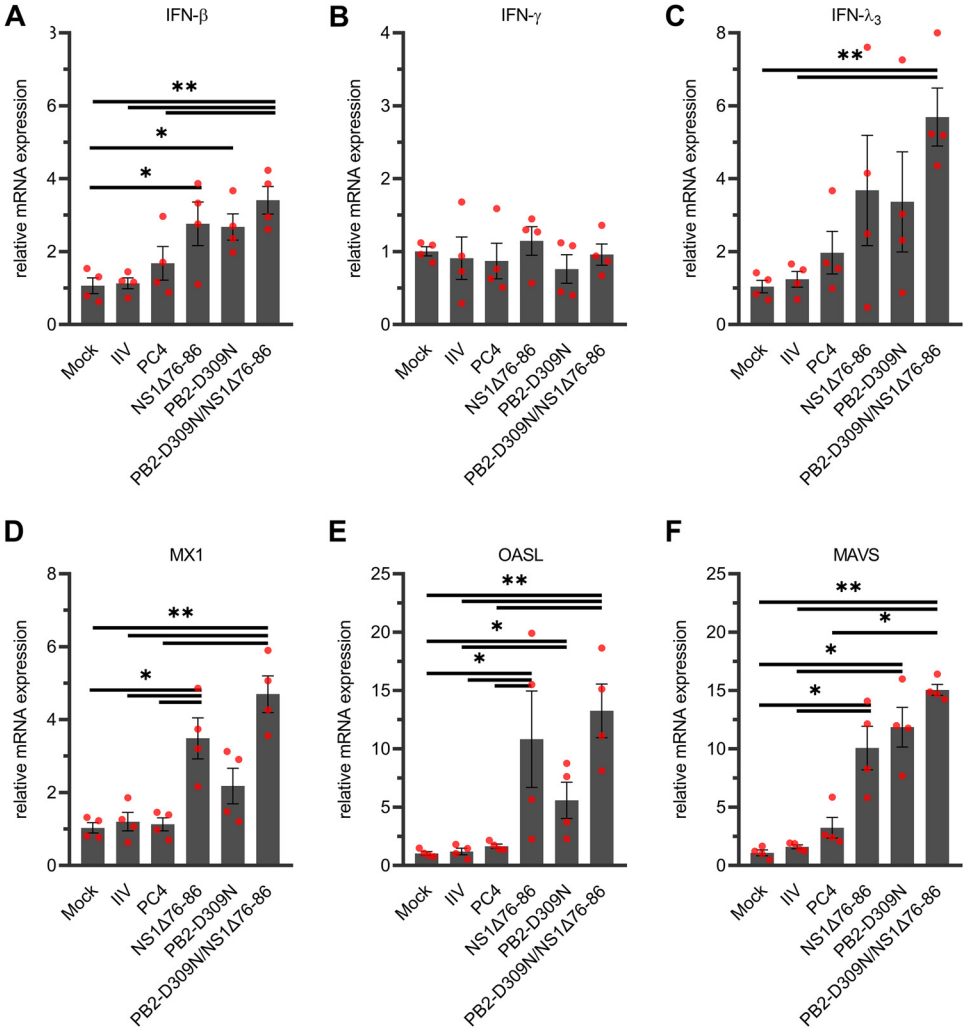


**FIG 8** Expression of IFN and IFN-related genes in vaccinated chickens. Two-week-old chickens were vaccinated with the PB2-D309N or NS1Δ76-86 single mutants, PB2-D309N/NS1Δ76-86 double mutant, or PC4 ($10^6$ $EID_{50}$/bird) via the intrachoanal and intraocular routes (1:1 ratio, vol/vol), injected subcutaneously with oil-adjuvanted inactivated PC4 vaccine (IIV), or left unvaccinated (mock). At 24 h postvaccination, chicken tracheas ($n = 4$/group) were collected, and the relative mRNA expression of IFN-$\beta$ (A), IFN-$\gamma$ (B), IFN-$\lambda_3$ (C), MX1 (D), OASL (E), and MAVS (F) genes in the tracheal tissue were determined using quantitative RT-PCR. Dots represent values for each individual chicken. Bars indicate mean ± SEM of chicken groups. **, $P < 0.01$; *, $P < 0.05$ (Kruskal-Wallis test).

in plaque-purified vesicular stomatitis virus (VSV) subpopulations by Marcus et al. (47), suggesting that minority HII subpopulations are commonly present in RNA viruses. Although these minority HII subpopulations are present in the parental populations, they are phenotypically outcompeted by the other subpopulations existing at higher thresholds. The HII phenotypes of PC4 clones were linked to the following two key mutations: PB2-D309N and NS1Δ76-86 (Table 1; Fig. 6). We combined these mutations to engineer a LAIV candidate with an exceptionally high ability to induce IFNs (Fig. 6 and 8) and stimulate a protective immunity in chickens (Fig. 9D). These results suggest that viral subpopulation-based screening in combination with deep sequencing can be instrumental in identifying rare immune-enhancing mutations for engineering novel LAIV candidates.

The PB2-D309N and NS1Δ76-86 mutations have additive effects on the enhancement of IFN responses (Fig. 6 and 7), which is in agreement with the nonredundant roles played by the NS1 and PB2 proteins in counteracting the activation of IFN production and signaling pathways (35, 44, 48). The NS1 protein employs a plethora of strategies to block or suppress multiple stages of the IFN pathway through direct

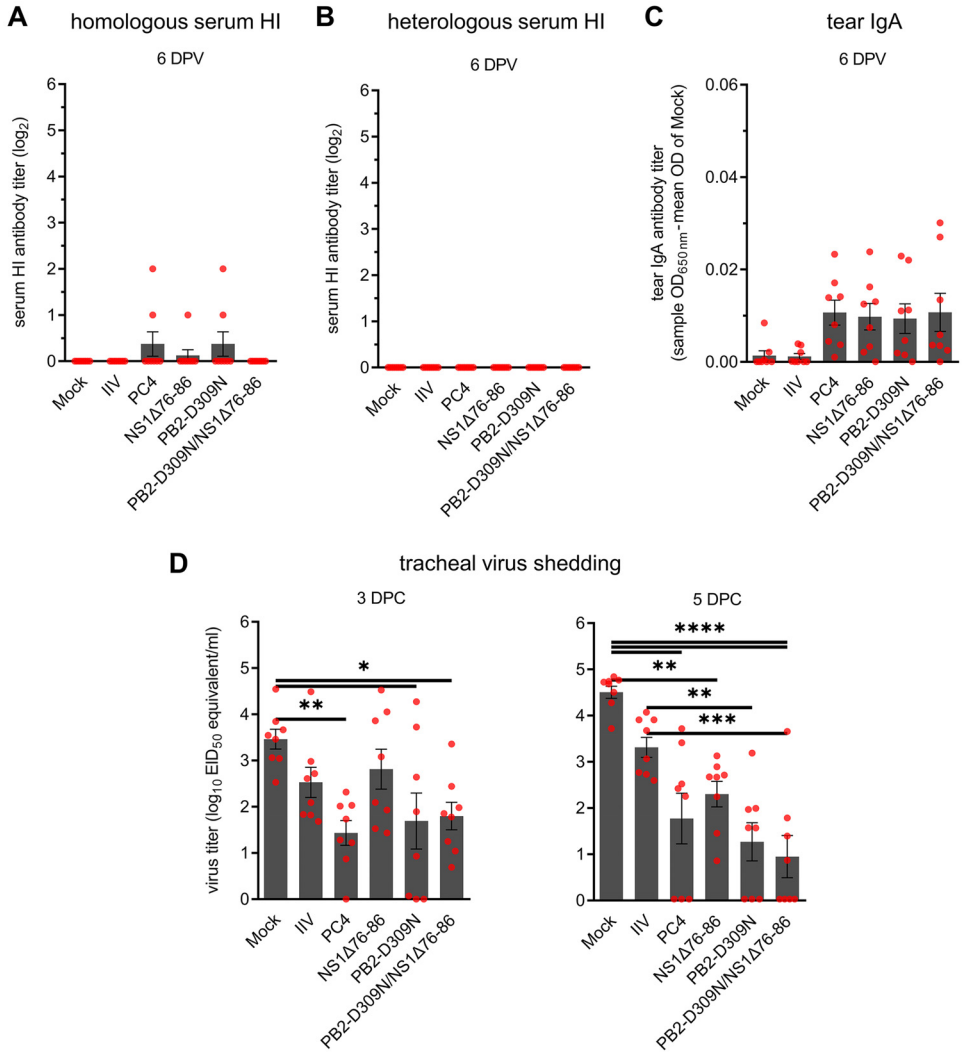


**FIG 9** Induction of humoral (A and B) and mucosal (C) antibodies and protective immunity (D) in vaccinated chickens. Two-week-old chickens were vaccinated as described in Fig. 8. (A) Homologous HI antibody titers in serum samples of vaccinated chickens at 6 days postvaccination (DPV; 1 day prior to challenge). (B) Heterologous HI antibody titers against the challenge virus antigen in serum samples of vaccinated chickens at 6 DPV. (C) Influenza virus-specific IgA antibody titers in chicken tears at 6 DPV as determined by a commercial IDEXX ELISA kit. IgA titers are shown as sample $OD_{650}$ minus the mean OD of mock. (D) Protective efficacies against the heterologous H7N2 challenge virus. At 7 DPV, chickens were challenged with an antigenically distant H7N2 virus ($10^6$ $EID_{50}$/bird), and the tracheal shedding of the virus was determined using quantitative RT-PCR at 3 and 5 DPC. Viral titers are expressed as $\log_{10}$ $EID_{50}$ equivalent per milliliters of the tracheal swab elutes (1 ml/swab). Dots represent values for individual chickens. Bars indicate mean ± SEM of chicken groups. ****, $P < 0.0001$; ***, $P < 0.001$; **, $P < 0.01$; *, $P < 0.05$ (one-way ANOVA with Tukey's *post hoc* test).

interaction with many cellular or viral factors, including different classes of RNAs (double-stranded RNA [dsRNA], mRNA, and snRNA) and host proteins (reviewed in references 15, 49). One such host protein is the eukaryotic translation initiation factor 4GI (eIF4GI), which interacts directly with amino acid residues 81 to 113 of the NS1 (50). The putative eIF4GI-binding domain of the NS1 encoded by PC4 is severely truncated (Fig. 4A) (24) and should, therefore, be incapable of blocking the translation of IFN mRNAs into biologically active proteins. Surprisingly, while the NS1Δ76-86 mutant induced similar amounts of IFN-$\beta$ mRNA as PC4 (Fig. 7A and C), its ability to block the synthesis of biologically active IFN was significantly abrogated (Fig. 7B). Based on the observation that the eIF4GI-binding activity in NS1 spans amino acid residues 81 to 113 (50) and the fact that the NS1Δ76-86 mutant is unable to block IFN mRNA translation

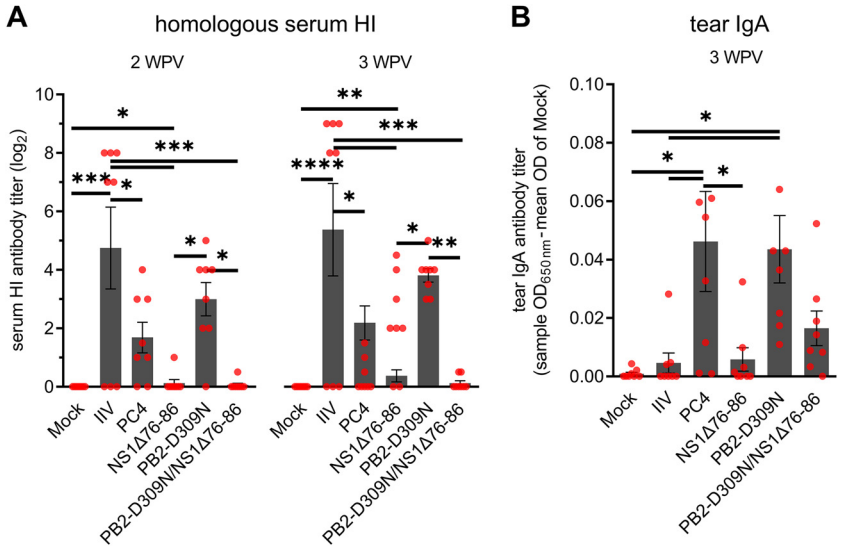


**FIG 10** Further progression of humoral (A) and mucosal (B) antibodies in vaccinated chickens. Chickens were vaccinated as described in Fig. 8. (A) Homologous HI antibody titers in serum samples of vaccinated chickens at 2 and 3 WPV. (B) Influenza virus-specific IgA antibody titers in chicken tears at 3 WPV as determined by a commercial IDEXX ELISA kit. IgA titers are shown as sample $OD_{650}$ minus the mean OD of mock. Dots represent values for individual chickens. Bars indicate mean ± SEM of chicken groups. ****, $P < 0.0001$; ***, $P < 0.001$; **, $P < 0.01$; *, $P < 0.05$ (one-way ANOVA with Tukey's *post hoc* test).

(this study), we propose that amino acids at positions 81 to 86 are indispensable for eIF4GI binding and suppression of IFN responses in avian cells.

The NS1 protein is scarcely present in virions, and new NS1 protein must be produced in infected cells to achieve sufficient antagonism of IFN responses (51). Here, we have demonstrated a novel role of the 309D residue of the PB2 protein in antagonism of IFN responses during the early stages of infection, before the production of new viral proteins begins. The PB2-309 residue is found in the midlink domain of the tripartite polymerase complex, in close proximity to the cap-binding domain (Fig. 4B) (52, 53), and is highly conserved among all avian influenza virus subtypes (Fig. 4C). Mechanistically, the PB2-309D residue is required to suppress the transcription of mRNAs given that the PB2-D309N substitution resulted in significant increase in IFN-$\beta$ mRNA transcription compared to that of PC4 (Fig. 7A and D to E). Furthermore, by blocking protein synthesis with cycloheximide, we showed that the PB2-309D proteins prepackaged in the incoming virions are sufficient to suppress IFN-$\beta$ transcription. Therefore, the PB2 protein plays a crucial role in suppressing IFN induction during the early stages of infection, potentially via a mechanism(s) requiring interaction of the PB2-309D residue with viral RNPs or cellular factors, such as $m^7G$ caps.

Previously, the PB2-D309N mutation was reported to emerge during serial passage of A/Puerto Rico/8/1934 (H1N1) viruses with mutated PB2 proteins (627V and 627A) at a temperature of 39°C in canine kidney epithelial MDCK cells but not in chicken embryo fibroblast DF-1 cells (40). The mutation was also demonstrated to enhance the activity of viral polymerase in human lung epithelial A549 cells but not the virus growth kinetics in human embryonic kidney HEK293T cells (40). Another study showed a G-to-D mutation at this position (PB2-G309D) to improve the replication of an avian H5N1 virus in A549 cells (54). While the apparent role of the PB2-309 residue in adaptation of IAVs in avian and mammalian hosts remains to be clarified, to our knowledge, our study is the first to link the PB2-D309N substitution with enhancement of innate immune responses in avian hosts.

We assessed whether the enhancement of innate immune responses by the PB2-D309N and NS1Δ76-86 mutations can translate to early protective immunity in chickens by challenging vaccinated birds at 1 WPV (Fig. 9D). One of the main concerns in development of IFN-inducing LAIV candidates is to achieve the right balance between

safety and immunogenicity (16). In general, NS1-truncated mutants with higher IFN-inducing abilities are more attenuated *in vivo*, resulting in poor induction of systemic serum antibodies (17, 19). Similarly, in our study, viruses with the NS1Δ76-86 mutation (PB2-D309N/NS1Δ76-86, NS1Δ76-86, HII-C2, and HII-C3 viruses) were characterized by smaller plaque sizes (Fig. 1E and 6C) and inefficiency in induction of serum HI antibodies relative to PC4 (Fig. 3A to C and Fig. 10). We speculate that this is due to reduced expression of viral proteins/antigens in infected cells because of a decrease in mRNA translation (see eIF4GI discussion above).

Interestingly, the PB2-D309N/NS1Δ76-86 double mutant was more protective than IIV during the peak of virus replication at 5 DPC (Fig. 9D) despite its poor serum HI antibody induction (Fig. 10). A discrepancy between serum antibody responses and the protective efficacy of LAIV has been reported in mice and humans (55, 56). Mucosal and systemic innate and cell-mediated responses are likely to be involved in the observed protection (57–62). The mechanism of protection by the double mutant virus may involve the accelerated production of types I and III IFNs ($\beta$ and $\lambda$, respectively) at the respiratory sites (Fig. 8A and C). Type I IFN was recently shown to enhance systemic antibody-mediated natural killer cell functions (63), while type III IFN (IFN-$\lambda$) was demonstrated to potentiate adaptive immune responses that initiate at mucosal surfaces (64). Furthermore, the LAIV-induced IFN could also neutralize the challenge virus by stimulating the development of an antiviral state.

Exaggerated induction of proinflammatory cytokines, commonly referred to as a "cytokine storm," is suggested to play a role in the immunopathology of highly pathogenic influenza viruses in chickens (65). This is linked to the ability of highly pathogenic influenza viruses to spread systemically to multiple body organs and infect multiple cell types, including epithelial, endothelial, and immune-related cells (66, 67). In sharp contrast, our NS1-truncated LAIVs localize and replicate to very low levels at the upper respiratory tract (24, 25). Even though these NS1-truncated LAIVs can potentially acquire a polybasic HA cleavage site like highly pathogenic influenza viruses, they are likely to be attenuated in chickens (68). We anticipate that the early induction of IFN responses by such NS1-truncated viruses can greatly inhibit virus replication at early stages of infection and, therefore, limit the associated immunopathology (65, 68).

In conclusion, our results showcase that subpopulation screening approaches can be used for simultaneous identification of rare mutations with potential immune-enhancing properties. However, the screening of plaque-purified subpopulations is labor-intensive, time-consuming, and may only reveal a limited number of mutations. Future studies may overcome these limitations by incorporating *in vitro* mutagenesis (69, 70) and high-throughput single-cell sorting (71–73) techniques to identify a larger pool of immune-enhancing mutations. Such mutations can then be combined to generate safer and more immunogenic live vaccine candidates as demonstrated in this study.

## MATERIALS AND METHODS

**Embryonated chicken eggs, cells, and viruses.** Embryonated chicken eggs (ECEs) were obtained from our on-site specific-pathogen-free flock of white leghorn chickens (Food Animal Health Research Program, The Ohio State University, Wooster, OH).

Primary CEF and chicken embryo kidney cells were freshly prepared from 10- and 18-day-old ECEs, respectively, as previously described (74). Freshly prepared primary cells were cultivated at 39°C and 5% $CO_2$ in RPMI 1640 medium (Gibco; catalog no. 11875135) supplemented with 10% fetal bovine serum (FBS) (Gibco; catalog no. 16000044), 10 $\mu$g/ml gentamicin (Gibco; catalog no. 15710072), and 0.25 $\mu$g/ml amphotericin B (Gibco; catalog no. 15290018). Developmentally aged CEF cells were prepared by allowing the freshly prepared CEF cells to grow for 10 days at 39°C and 5% $CO_2$ in RPMI medium containing 5% FBS, 10 $\mu$g/ml gentamicin, and 0.25 $\mu$g/ml amphotericin B as previously described (30, 33, 34, 75). QT-35 cells (ECACC; catalog no. 93120832) were maintained at 37°C and 5% $CO_2$ in minimum essential medium (MEM) (Gibco; catalog no. 11095080) containing 10% FBS and 10 $\mu$g/ml gentamicin. Human embryonic kidney 293T (HEK293T) (ATCC; catalog no. CRL-3216) cells were maintained at 37°C and 5% $CO_2$ in Dulbecco's modified Eagle's medium (DMEM) (Gibco; catalog no. 12430062) supplemented with 10% FBS and 10 $\mu$g/ml gentamicin.

The A/turkey/OR/71 (H7N3) virus strains encoding full-size (wild type) or truncated (PC4) NS1 proteins were generated by using reverse genetics (24) and propagated in 10-day-old ECEs. The A/chicken/NJ/150383-7/02 (H7N2) virus, which was used as the heterologous challenge virus in chicken experiments, was obtained from the repository of the Food Animal Health Research Program (Wooster, OH).

**Virus plaque purification and titration.** Clonal virus populations were plaque purified in CEF cells and grown in 10-day-old ECEs. Briefly, freshly prepared CEF cells were seeded in 6-well plates at a density of $2 \times 10^6$ cells/well and allowed to grow to confluence overnight. Confluent monolayers were washed twice with RPMI medium (prewarmed to 37°C) before being infected with 200 $\mu$l of inoculums containing ~1 to 5 PFU of a given virus per well. Virus attachment was done at 37°C for 60 min in the $CO_2$ incubator, with rocking of the plates every 15 min. At the end of the virus attachment, the plates were washed one more time with RPMI medium and overlaid with a medium containing MEM plus 0.6% agarose and 0.4 $\mu$g/ml tosylsulfonyl phenylalanyl chloromethyl ketone, L-1-tosylamide-2-phenylmethyl chloromethyl ketone (TPCK)-treated trypsin. To visualize the plaques, 1 ml of a second overlay medium containing MEM, 0.6% agarose, and 50 $\mu$g/ml of neutral red dye was added to each well at 48 hpi, and the plates were incubated at 37°C in the $CO_2$ incubator overnight for live cells to absorb the neutral red dye. Individual plaques were picked using sterile pipette tips, eluted in 1 ml of sterile phosphate-buffered saline (PBS) (Gibco; catalog no. 70011069) supplemented with 10 $\mu$g/ml gentamicin and propagated by inoculating five 10-day-old ECEs (0.2 ml/egg) per each plaque via allantoic cavity route. ECEs were then incubated for 72 to 96 h at 37°C with daily monitoring of embryo viability. Allantoic fluid from each ECE was harvested and tested for hemagglutination activity to determine the presence of virus. Infectious allantoic fluids with positive hemagglutination results were pooled, clarified by centrifugation at $5{,}000 \times g$ for 20 min, aliquoted into 2-ml tubes, and stored at −70°C until being used for experiments.

Virus titration was performed through plaque assay of serial 10-fold virus dilutions in chicken embryo kidney cells, in triplicate for each virus dilution. The infected cell monolayers were incubated at 37°C for 60 h, fixed with 10% formalin, and stained with 0.1% crystal violet for 3 to 5 min to visualize the plaques. Plaque images were captured using the FluorChem Q imaging system (Alpha Innotech; catalog no. 92-14095-00) and plaque diameters measured using ImageJ software (National Institutes of Health; http://imagej.nih.gov/ij).

**Induction and purification of acid-stable type I IFN.** Induction of biologically active IFN was performed in developmentally aged CEF cell monolayers as previously described (30, 33, 34, 75). Briefly, freshly prepared CEF cells were seeded in 6-well plates at a density of $1 \times 10^6$ cells/well and allowed to grow in RPMI medium supplemented with 5% FBS for 10 days. On average, each developmentally aged CEF cell monolayer contained $5 \times 10^6$ cells/well at the time of infection. The cell monolayers were infected in triplicate with the designated viruses at an MOI of 0.3 PFU per cell, which was shown to induce the peak IFN response (Fig. 1B). Following virus attachment for 1 h, 1 ml of fresh RPMI medium (without trypsin) was added to each well. Cell culture supernatants were harvested at 24 hpi and kept on ice until being used in the next step.

Acid-stable type I IFNs in the cell supernatants were partially purified through precipitation of acid-labile proteins with perchloric acid ($HClO_4$; final concentration of 0.15 M) at 4°C overnight. Precipitated proteins were removed by centrifugation at $2{,}000 \times g$ for 10 min. The clarified supernatants were neutralized with KOH and placed on ice for 1 h to allow the $KClO_4$ salts to precipitate. The supernatants containing type I IFNs were then gently decanted into final tubes and preserved at −20°C until being tested.

**Quantification of antiviral activity of IFN.** QT-35 cells were seeded in black-wall 96-well plates at a density of $2 \times 10^4$ cells/well in MEM supplemented with 10% FBS and allowed to grow to confluence for 48 h at 37°C in a $CO_2$ incubator. Confluent cell monolayers were treated by increasing amounts of the purified IFNs in MEM plus 1% FBS for 18 to 20 h at 37°C. The supernatant medium was then replaced with MEM containing vesicular stomatitis virus that expresses green fluorescent protein (GFP) (VSV-GFP) (kindly provided by Jianrong Li, The Ohio State University, Columbus, OH) (76) at an MOI of 1 PFU per cell. The intensity of fluorescence light emitted from each well of the 96-well plate was measured by the GloMax-Multi detection system (Promega; catalog no. E7081) using blue fluorophore (excitation, 490 nm; emission, 510 to 570 nm) at 24 hpi. After subtracting the average background intensity from all wells, percent inhibitory activities were determined by comparing the signal intensities from IFN-treated wells with the average intensities recorded for mock-treated infected controls. The antiviral activities were extrapolated as IFN units per milliliter using recombinant chicken IFN-$\alpha$ (Bio-Rad Antibodies; catalog no. PAP004) as a standard. In this assay, one unit of IFN consistently provided a 50% inhibitory activity against VSV-GFP. Relative antiviral activities were calculated by dividing the IFN units induced by the tested samples by the average IFN units induced by PC4 controls in the same experiment. To perform the IFN bioassay on samples derived from cells treated with cycloheximide (Sigma; catalog no. C7698), the cell supernatants were prediluted 1,000-fold to prevent the inhibitory activity of cycloheximide on the assay.

**Deep sequencing and sequence analysis.** Viral RNA was extracted from 100 $\mu$l of allantoic fluids (virus stocks) using the QIAamp viral RNA minikit (Qiagen; catalog no. 52906) following the manufacturer's instructions. Amplification of IAV genome, including cDNA synthesis and PCR, was performed as previously described (77). Briefly, cDNA synthesis was performed on 3 $\mu$l of viral RNA for each sample using SuperScript IV reverse transcriptase (Invitrogen; catalog no. 18090050) with MBTuni-12 primer (5′-ACGCGTGATCAGCAAAAGCAGG-3′). PCR amplification was performed on 5 $\mu$l of prediluted cDNA, containing $4 \times 10^6$ genome copies (estimated based on influenza matrix gene copies), using high-fidelity Phusion polymerase (NEB; catalog no. M0530S) with MBTuni-13 (5′-ACGCGTGATCAGTAGAAACAAGG-3′) and MBTuni-12 (5′-ACGCGTGATCAGCAAAAGCAGG-3′) primers. The PCR conditions used were 98°C for

30 s followed by 25 cycles of 98°C for 10 s, 57°C for 30 s, and 72°C for 90 s; a terminal extension of 72°C for 5 min; and a final 10°C hold. PCR products were purified using the PureLink PCR purification kit (Invitrogen; catalog no. K310001) with the lower cutoff option (buffer B2) and eluted in 30 $\mu$l distilled water (dH2O). Purified PCR products were used for library preparation using Kapa HyperPrep kit (Roche) and deep sequenced on the Illumina MiSeq platform (paired-end 2 $\times$ 250 bp chemistry) at the University of Minnesota Genomics Center (Minneapolis, MN). Analysis of consensus sequences and minor single-nucleotide variants within each virus population was performed using the web-based INSaFLU suite of bioinformatics tools (78). Consensus sequences were confirmed using the FLU module of the CDC's Iterative Refinement Meta-Assembler (IRMA; version 0.9.2) pipeline (79) using the high-performance computing resources provided by the Ohio Supercomputer Center (Columbus, OH). Mean depth of coverage for all segments of influenza genome across all sequenced samples was equal to 5,664 with minimum average coverage being >1,000 for all segments. To confirm the deletions in NS1 protein, NS genes were PCR amplified using MBTuni-13 and MBTuni-12 primers and visualized on 1.5% agarose gel. PCR products were then extracted from the agarose gel using QIAquick gel extraction kit (Qiagen; catalog no. 28706), cloned into pCR2.1-TOPO vector (Invitrogen; catalog no. K450040), and amplified in Stellar competent cells (TaKaRa Bio; catalog no. 636763) as previously described (80). Amplified plasmid DNA was extracted using the QIAprep spin miniprep kit (Qiagen; catalog no. 27106) and Sanger sequenced at the Molecular and Cellular Imaging Center (MCIC), The Ohio State University (Wooster, OH). The PB2-309N residue was plotted on the influenza virus polymerase complex crystal structure (PDB accession number 6T0V) by using the PyMOL molecular graphics system (version 2.3.2; Schrödinger, LLC). The number of avian influenza virus strains possessing different amino acids at position 309 of PB2 protein or deletion at position 76 to 86 of NS1 protein was determined using the "Analyze Sequence Variation (SNP)" tool in the National Institute of Allergy and Infectious Diseases (NIAID) Influenza Research Database (accessed 16 April 2020) (42).

**Construction of plasmids encoding the mutated NS and PB2 gene segments.** The mutant NS gene was amplified from the HII-C3 plaque clone and cloned into the pHH21 vector between the promoter and terminator sequences of RNA polymerase I as previously described (80, 81). A pHH21 plasmid encoding a mutated PB2 segment with the D309N mutation was constructed using site-directed mutagenesis. The PB2-D309N mutation was generated using overlap extension PCR with Phusion polymerase (NEB; catalog no. M0530S) (82) and the following mismatched primers: PB2-G952A-F, 5′-GAGGAACAAGCCGTGAATATATGCAAGGCAGCAATGGGCTTGAGGATTAGC-3′; PB2-G952A-R, 5′-GCTGCC TTGCATATATTCACGGCTTGTTCCTCTGTTGGATTCTGCCTAAGG-3′. Briefly, 1 ng of the original pHH21 plasmid was used as template DNA to perform a standard 50-$\mu$l PCR using Phusion polymerase according to the following thermal program: initial denaturation of 98°C for 30 s; then 20 cycles of 98°C for 10 s, 60°C for 30 s, and 72°C for 6 min; and final extension at 72°C for 5 min. After PCR, 1 $\mu$l of DpnI restriction enzyme was directly added to the reaction tube and incubated at 37°C for 2 h to digest the original unmutated plasmids. The DpnI-digested PCR product was purified using QIAquick gel extraction kit. Finally, 2.5 $\mu$l of the purified PCR product was used to transform 25 $\mu$l of Stellar competent cells (TaKaRa Bio; catalog no. 636763). Extraction of plasmid DNA from positive bacterial clones was performed using the QIAprep spin miniprep kit (Qiagen; catalog no. 27106).

**Rescue of recombinant viruses.** Recombinant viruses were rescued using a 12-plasmid-based reverse genetics system as previously described (80, 81). Briefly, HEK293T cells were transfected with 0.4 $\mu$g of each of the 8 transcription plasmids and 0.6 $\mu$g of four expression plasmids (PB2, PB1, PA, and NP from A/WSN/33 [kindly provided by Yoshihiro Kawaoka, University of Wisconsin, WI]) with the use of Lipofectamine 3000 reagent (Invitrogen; catalog no. L3000008). The transcription plasmids (pHH21) encoding all segments of the A/turkey/OR/71 (H7N3) strain were described previously (24). Forty-eight hours after transfection, the supernatant medium was collected and inoculated into five 10-day-old ECEs (0.2 ml/egg) per transfected cell monolayer. ECEs were then incubated for 72 to 96 h at 37°C with daily monitoring of embryo viability. Allantoic fluid from each ECE was harvested and tested for hemagglutination activity to determine the presence of virus. Infectious allantoic fluids containing the recombinant viruses were harvested, centrifuged at 5,000 $\times$ *g* for 20 min to remove the egg-derived debris, decanted in new tube, and stored at −70°C until use. Mutations in the modified virus segments were confirmed by Sanger sequencing. Briefly, viral RNA was extracted from 100 $\mu$l of virus stocks using QIAamp viral RNA minikit. Then, 5 $\mu$l of 1:50 diluted viral RNAs was reverse transcribed and amplified using a OneStep reverse transcriptase PCR (RT-PCR) kit (Qiagen; catalog no. 210212) with segment-specific primer sets. Amplified DNA products were extracted from the agarose gel using QIAquick gel extraction kit and Sanger sequenced at the MCIC, The Ohio State University (Wooster, OH).

**Chicken experiments.** Two-week-old white leghorn chickens were obtained from our on-site specific-pathogen-free flock (Food Animal Health Research Program, The Ohio State University, Wooster, OH). The chickens were housed in a biosafety level 2 (BSL2) facility with HEPA-filtered forced air ventilation. The birds were kept inside polyethylene molded isolators (Federal Designs Inc.; model no. 934-1) for the duration of the experiment. The care, management, and euthanasia of chickens were performed as previously reported in detail (26, 27).

At 2 weeks of age, the birds were vaccinated with candidate LAIVs or IIV. Vaccination with the parental PC4 or other HII viruses was done via intraocular and intrachoanal routes (1:1 ratio, vol/vol) at a dose of $10^6$ 50% egg infective dose ($EID_{50}$) per bird (in 0.2 ml total volume). IIV was delivered via the subcutaneous route with 0.5 ml of $\beta$-propiolactone-inactivated PC4 virus preparation mixed with Montanide ISA 70 VG adjuvant (Seppic, Paris, France; virus/adjuvant, 3:7 vol/vol ratio, ~1,152 hemagglutinating units/dose). Mock groups remained unvaccinated and uninfected prior to challenge. At 1 or 3

**TABLE 2** Primers used for transcriptional analysis of innate immune responses

| Primer name | Sequence (5′→3′) | Reference |
|---|---|---|
| IFN-$\beta$ for | ACAACTTCCTACAGCACAACAACTA | 85 |
| IFN-$\beta$ rev | GCCTGGAGGCGGACATG | |
| IFN-$\gamma$ for | CAAGTCAAAGCCGCACATC | 86 |
| IFN-$\gamma$ rev | CGCTGGATTCTCAAGTCGTT | |
| IFN-$\lambda_3$ for | GGAGGATGAAGGAGCAGTTTG | 87 |
| IFN-$\lambda_3$ rev | ACGGTGATGGTGAGGTCC | |
| MX1 for | ATCCATGGTCCAACTTCAGC | 88 |
| MX1 rev | GCCTCTTGGACACTTTCTGC | |
| OASL for | CACGGCCTCTTCTACGACA | 89 |
| OASL rev | TGGGCCATACGGTGTAGACT | |
| MAVS for | CACCCACGAGGTCCATGTG | 90 |
| MAVS rev | TGCTTCATCTGGGACATCATTG | |
| GAPDH for | CCCCAATGTCTCTGTTGTTGAC | 85 |
| GAPDH rev | CAGCCTTCACTACCCTCTTGAT | |

WPV, the birds were challenged intrachoanally with heterologous A/chicken/NJ/150383-7/02 (H7N2) virus ($10^6$ $EID_{50}$ per bird in 0.2 ml total volume) depending on the experiment.

Blood and tear samples were collected as previously described in detail (26, 27). Serum HI antibody titers were determined using 2-fold serially diluted serum samples, 8 hemagglutinating units of live PC4 virus antigens, and 1% turkey erythrocyte suspension (26, 27). Tear IgA titers were measured using commercial avian influenza virus IDEXX AI Ab test enzyme-linked immunosorbent assay (ELISA) kit (IDEXX; catalog no. 99-09269) using 1:10,000 dilution of horseradish peroxidase (HRP)-labeled alpha-chain-specific goat-anti-chicken IgA conjugates (Gallus Immunotech Inc.; catalog no. 60220) as the secondary antibody (26, 27).

Tracheal shedding of the challenge virus was determined through quantification of viral RNA in tracheal swabs collected at 3 and 5 DPC as previously described (26, 27, 83). Tracheal swabs (Puritan; catalog no. 25-3316-U) were eluted into 1 ml of PBS supplemented with gentamicin (10 $\mu$g/ml). Viral RNA was extracted from 100 $\mu$l of the supernatant using QIAamp viral RNA minikit. Quantification of viral RNA was done through quantitative RT-PCR using primers and probes specifically designed for influenza A virus matrix gene (83). Tracheal virus shedding titers were calculated as $EID_{50}$ equivalents per milliliter of swab elutes based on the cycle threshold values in quantitative RT-PCR as previously described (26, 27, 83).

**Transcriptional analysis of innate immune responses.** To evaluate the relative expression of IFN-$\beta$ mRNA in infected cells, QT-35 cell monolayers were seeded in 6-well plates at a density of $1 \times 10^6$ cells/well and allowed to grow overnight. Cell monolayers were infected with the virus at an MOI of 0.3 PFU per cell. Following virus attachment for 1 h, 2 ml of fresh MEM (without trypsin) was added to each well. The supernatant medium was then replaced with 500 $\mu$l of TRIzol reagent (Invitrogen; catalog no. 15596018) per each well of a 6-well plate at the indicated time points after infection. The cell lysates were collected into sterile 2-ml tubes and preserved at −70°C until RNA extraction. When required, cycloheximide was added into the cell medium 30 min before infection and throughout the infection period at 50 $\mu$g/ml (44).

For transcriptional analysis in vaccinated chickens, a small (~0.5 cm long) section of upper trachea was collected in 1 ml of TRIzol reagent at 24 hpi. Samples were stored at −70°C until further processing. Tracheal tissues were then homogenized in ZR BashingBead lysis tubes (Zymo Research; catalog no. S6012-50) using TissueLyser II (Qiagen; catalog no. 85300). To remove the bulk of genomic DNA in homogenized tissues, 200 $\mu$l of chloroform was added to each tube, the tubes were then centrifuged at 16,000 $\times$ *g* for 20 min, and the transparent layer of the supernatant was used for RNA extraction.

Total RNA was extracted using Direct-zol RNA miniprep plus kit (Zymo Research; catalog no. R2071) following the manufacturer's instructions. mRNA was reverse transcribed into cDNA using GoScript reverse transcriptase (Promega; catalog no. A5001) with oligo$(dT)_{15}$ primer. Briefly, 10 $\mu$l of RNA (80 ng/$\mu$l) was mixed with 2 $\mu$l of 1:3 diluted oligo$(dT)_{15}$ primer (500 ng/$\mu$l), incubated at 72°C for 5 min, and immediately placed on ice. Then, 8 $\mu$l of master mix containing 4 $\mu$l of 5$\times$ buffer, 2 $\mu$l of $MgCl_2$, 1 $\mu$l of deoxynucleoside triphosphate (dNTP) mix, and 1 $\mu$l of reverse transcriptase enzyme was added to each tube and cDNA synthesis was allowed to take place at 42°C for 1 h. Quantitative PCR was performed using PerfeCTa SYBR green fastmix (QuantaBio; catalog no. 95074-012) in a 7500 real-time PCR system (Applied Biosystems; catalog no. 4351105). Briefly, 5 $\mu$l of the 1:5 diluted cDNA was mixed with 15 $\mu$l of master mix containing 10 $\mu$l of the SYBR green mix and 2.5 $\mu$l of each primer (20 $\mu$M) in a 0.2-ml tube. The cycle conditions of quantitative PCR were 95°C for 10 min, followed by 40 cycles of 95°C for 15 s and 60°C for 1 min. Afterward, melting curve analysis was performed from 60°C to 90°C. The primer sequences used for transcriptional analysis are listed in Table 2. Differential gene expressions were normalized using chicken glyceraldehyde-3-phosphate dehydrogenase (GAPDH) gene as the internal control. Relative mRNA expression levels were calculated as fold changes over the mock group using the $2^{-\Delta\Delta CT}$ method (84).

**Statistical analysis and data visualization.** Statistical analysis and data visualization were performed using GraphPad Prism version 8 (GraphPad Software, San Diego, CA). Statistically significant differences of gene expressions in chicken tracheas were assessed by using the Kruskal-Wallis test.

Statistical analyses in all other experiments were performed through two-tailed unpaired *t* test (for two groups) and one-way analysis of variance (ANOVA) followed by Tukey's *post hoc* test (for more than two groups). A $P$ value of $<0.05$ was considered significantly different.

**Ethics statement.** All experimental animals were handled according to protocol no. 2009AG0002 approved by The Ohio State University Institutional Animal Care and Use Committee (IACUC). This protocol follows the U.S. Animal Welfare Act, Guide for Care and Use of Laboratory Animals, and Public Health Service Policy on Humane Care and Use of Laboratory Animals. The Ohio State University is accredited by the Association for the Assessment and Accreditation of Laboratory Animal Care International (AAALAC).

**Data availability.** Sequence data have been deposited in the NCBI GenBank and Sequence Read Archive (SRA) databases. The consensus sequences of the plaque clones and PC4 are available in GenBank under accession numbers MW080971 to MW081050. The raw deep-sequence reads are available under BioProject number PRJNA668426 and Sequence Read Archive (SRA) numbers SRX9274256 to SRX9274266, respectively. All data from this study are fully available without any restrictions.

## ACKNOWLEDGMENTS

We acknowledge the professional and enthusiastic support from our animal care team, Juliette Hanson, Megan Strother, Jane Cooper, Sara Tallmadge, Ronna Wood, and Dennis Hartzler.

This project was supported by Agriculture and Food Research Initiative competitive grant no. 2013-67015-20476 from the U.S. Department of Agriculture National Institute of Food and Agriculture and funds appropriated to the Ohio Agricultural Research and Development Center, The Ohio State University.

C.-W.L., J.M.N., and A.G. developed the broad concept of the study. A.G., C.-W.L., and J.M.N. designed and managed the study. A.G. performed the lab experiments, sample processing, and bioinformatics analyses. A.G., M.C.A., J.M.N., H.J., and K.J.M.T. performed the chicken experiments including animal husbandry and treatment, necropsy, and collection and processing of samples. C.-W.L. provided all of the reagents and resources. A.G. wrote the first draft of the manuscript. All authors read, corrected, and approved the final manuscript.

We declare no conflict of interest.

## REFERENCES

1. Eisfeld AJ, Neumann G, Kawaoka Y. 2015. At the centre: influenza A virus ribonucleoproteins. Nat Rev Microbiol 13:28–41. https://doi.org/10.1038/nrmicro3367.
2. Ghorbani A, Ngunjiri JM, Lee C-W. 2020. Influenza A virus subpopulations and their implication in pathogenesis and vaccine development. Annu Rev Anim Biosci 8:247–267. https://doi.org/10.1146/annurev-animal-021419-083756.
3. Domingo E, Sheldon J, Perales C. 2012. Viral quasispecies evolution. Microbiol Mol Biol Rev 76:159–216. https://doi.org/10.1128/MMBR.05023-11.
4. Brooke CB. 2017. Population diversity and collective interactions during influenza virus infection. J Virol 91:e01164-17. https://doi.org/10.1128/JVI.01164-17.
5. Neumann G, Kawaoka Y. 2019. Predicting the next influenza pandemics. J Infect Dis 219:S14–S20. https://doi.org/10.1093/infdis/jiz040.
6. Yoon S-W, Webby RJ, Webster RG. 2014. Evolution and ecology of influenza A viruses, p 359–375. *In* Compans RW, Oldstone MBA (ed), Influenza pathogenesis and control, vol 1. Springer, Cham, Switzerland.
7. Donatelli I, Castrucci MR, De Marco MA, Delogu M, Webster RG. 2017. Human–animal interface: the case for influenza interspecies transmission, p 17–33. *In* Rezza G, Ippolito G (ed), Emerging and re-emerging viral infections: advances in microbiology, infectious diseases and public health, vol 6. Springer, Cham, Switzerland.
8. Xu Y, Ramey AM, Bowman AS, DeLiberto TJ, Killian ML, Krauss S, Nolting JM, Torchetti MK, Reeves AB, Webby RJ, Stallknecht DE, Wan X-F. 2017. Low-pathogenic influenza A viruses in North American diving ducks contribute to the emergence of a novel highly pathogenic influenza A (H7N8) virus. J Virol 91:e02208-16. https://doi.org/10.1128/JVI.02208-16.
9. Swayne DE, Hill RE, Clifford J. 2017. Safe application of regionalization for trade in poultry and poultry products during highly pathogenic avian influenza outbreaks in the USA. Avian Pathol 46:125–130. https://doi.org/10.1080/03079457.2016.1257775.
10. Swayne DE. 2020. Laboratory methods for assessing and licensing influenza vaccines for poultry, p 211–225. *In* Spackman E (ed), Animal influenza virus: methods and protocols. Springer, New York, NY.
11. Erbelding EJ, Post DJ, Stemmy EJ, Roberts PC, Augustine AD, Ferguson S, Paules CI, Graham BS, Fauci AS. 2018. A universal influenza vaccine: the strategic plan for the National Institute of Allergy and Infectious Diseases. J Infect Dis 218:347–354. https://doi.org/10.1093/infdis/jiy103.
12. Iwasaki A, Pillai PS. 2014. Innate immunity to influenza virus infection. Nat Rev Immunol 14:315–328. https://doi.org/10.1038/nri3665.
13. Ramos I, Carnero E, Bernal-Rubio D, Seibert CW, Westera L, Garcia-Sastre A, Fernandez-Sesma A. 2013. Contribution of double-stranded RNA and CPSF30 binding domains of influenza virus NS1 to the inhibition of type I interferon production and activation of human dendritic cells. J Virol 87:2430–2440. https://doi.org/10.1128/JVI.02247-12.
14. Phipps-Yonas H, Seto J, Sealfon SC, Moran TM, Fernandez-Sesma A. 2008. Interferon-$\beta$ pretreatment of conventional and plasmacytoid human dendritic cells enhances their activation by influenza virus. PLoS Pathog 4:e1000193. https://doi.org/10.1371/journal.ppat.1000193.
15. Rosário-Ferreira N, Preto AJ, Melo R, Moreira IS, Brito RM. 2020. The central role of non-structural protein 1 (NS1) in influenza biology and infection. Int J Mol Sci 21:1511. https://doi.org/10.3390/ijms21041511.
16. Richt JA, García-Sastre A. 2009. Attenuated influenza virus vaccines with modified NS1 proteins, p 177–195. *In* Compans RW, Orenstein WA (ed), Vaccines for pandemic influenza. Springer-Verlag, Heidelberg, Germany.
17. Talon J, Salvatore M, O'Neill RE, Nakaya Y, Zheng H, Muster T, Garcia-Sastre A, Palese P. 2000. Influenza A and B viruses expressing altered NS1 proteins: a vaccine approach. Proc Natl Acad Sci U S A 97:4309–4314. https://doi.org/10.1073/pnas.070525997.
18. Falcon AM, Fernandez-Sesma A, Nakaya Y, Moran TM, Ortin J, Garcia-Sastre A. 2005. Attenuation and immunogenicity in mice of temperature-sensitive influenza viruses expressing truncated NS1 proteins. J Gen Virol 86:2817–2821. https://doi.org/10.1099/vir.0.80991-0.
19. Solórzano A, Webby RJ, Lager KM, Janke BH, García-Sastre A, Richt JA. 2005. Mutations in the NS1 protein of swine influenza virus impair

anti-interferon activity and confer attenuation in pigs. J Virol 79:7535–7543. https://doi.org/10.1128/JVI.79.12.7535-7543.2005.
20. Richt JA, Lekcharoensuk P, Lager KM, Vincent AL, Loiacono CM, Janke BH, Wu W-H, Yoon K-J, Webby RJ, Solórzano A, García-Sastre A. 2006. Vaccination of pigs against swine influenza viruses by using an NS1-truncated modified live-virus vaccine. J Virol 80:11009–11018. https://doi.org/10.1128/JVI.00787-06.
21. Vincent AL, Ma W, Lager KM, Janke BH, Webby RJ, Garcia-Sastre A, Richt JA. 2007. Efficacy of intranasal administration of a truncated NS1 modified live influenza virus vaccine in swine. Vaccine 25:7999–8009. https://doi.org/10.1016/j.vaccine.2007.09.019.
22. Quinlivan M, Zamarin D, García-Sastre A, Cullinane A, Chambers T, Palese P. 2005. Attenuation of equine influenza viruses through truncations of the NS1 protein. J Virol 79:8431–8439. https://doi.org/10.1128/JVI.79.13.8431-8439.2005.
23. Chambers TM, Quinlivan M, Sturgill T, Cullinane A, Horohov DW, Zamarin D, Arkins S, García-Sastre A, Palese P. 2009. Influenza A viruses with truncated NS1 as modified live virus vaccines: pilot studies of safety and efficacy in horses. Equine Vet J 41:87–92. https://doi.org/10.2746/042516408x371937.
24. Wang L, Suarez D, Pantin-Jackwood M, Mibayashi M, Garcia-Sastre A, Saif Y, Lee C-W. 2008. Characterization of influenza virus variants with different sizes of the non-structural (NS) genes and their potential as a live influenza vaccine in poultry. Vaccine 26:3580–3586. https://doi.org/10.1016/j.vaccine.2008.05.001.
25. Jang H, Ngunjiri JM, Lee C-W. 2016. Association between interferon response and protective efficacy of NS1-truncated mutants as influenza vaccine candidates in chickens. PLoS One 11:e0156603. https://doi.org/10.1371/journal.pone.0156603.
26. Jang H, Elaish M, Kc M, Abundo MC, Ghorbani A, Ngunjiri JM, Lee CW. 2018. Efficacy and synergy of live-attenuated and inactivated influenza vaccines in young chickens. PLoS One 13:e0195285. https://doi.org/10.1371/journal.pone.0195285.
27. Ghorbani A, Ngunjiri JM, Xia M, Elaish M, Jang H, Mahesh KC, Abundo MC, Jiang X, Lee CW. 2019. Heterosubtypic protection against avian influenza virus by live attenuated and chimeric norovirus P-particle-M2e vaccines in chickens. Vaccine 37:1356–1364. https://doi.org/10.1016/j.vaccine.2019.01.037.
28. Baskin CR, Bielefeldt-Ohmann H, Garcia-Sastre A, Tumpey TM, Van Hoeven N, Carter VS, Thomas MJ, Proll S, Solorzano A, Billharz R, Fornek JL, Thomas S, Chen CH, Clark EA, Murali-Krishna K, Katze MG. 2007. Functional genomic and serological analysis of the protective immune response resulting from vaccination of macaques with an NS1-truncated influenza virus. J Virol 81:11817–11827. https://doi.org/10.1128/JVI.00590-07.
29. Nicolodi C, Groiss F, Kiselev O, Wolschek M, Seipelt J, Muster T. 2019. Safety and immunogenicity of a replication-deficient H5N1 influenza virus vaccine lacking NS1. Vaccine 37:3722–3729. https://doi.org/10.1016/j.vaccine.2019.05.013.
30. Marcus PI, Ngunjiri JM, Sekellick MJ, Wang L, Lee CW. 2010. *In vitro* analysis of virus particle subpopulations in candidate live-attenuated influenza vaccines distinguishes effective from ineffective vaccines. J Virol 84:10974–10981. https://doi.org/10.1128/JVI.00502-10.
31. Ngunjiri JM, Ali A, Boyaka P, Marcus PI, Lee C-W. 2015. In vivo assessment of NS1-truncated influenza virus with a novel SLSYSINWRH motif as a self-adjuvanting live attenuated vaccine. PLoS One 10:e0118934. https://doi.org/10.1371/journal.pone.0118934.
32. Ngunjiri JM, Lee C-W, Ali A, Marcus PI. 2012. Influenza virus interferon-inducing particle efficiency is reversed in avian and mammalian cells, and enhanced in cells co-infected with defective-interfering particles. J Interferon Cytokine Res 32:280–285. https://doi.org/10.1089/jir.2011.0102.
33. Sekellick MJ, Biggers WJ, Marcus PI. 1990. Development of the interferon system. I. In chicken cells development in ovo continues on time in vitro. In Vitro Cell Dev Biol 26:997–1003. https://doi.org/10.1007/BF02624475.
34. Sekellick MJ, Marcus PI. 1986. Induction of high titer chicken interferon, p 115–125. *In* Pestka S (ed), Methods in enzymology, vol 119. Elsevier, Cambridge, MA.
35. Marcus PI, Rojek JM, Sekellick MJ. 2005. Interferon induction and/or production and its suppression by influenza A viruses. J Virol 79:2880–2890. https://doi.org/10.1128/JVI.79.5.2880-2890.2005.
36. DeGrado WF, Wasserman ZR, Chowdhry V. 1982. Sequence and structural homologies among type I and type II interferons. Nature 300:379–381. https://doi.org/10.1038/300379a0.
37. Rentsch MB, Zimmer G. 2011. A vesicular stomatitis virus replicon-based bioassay for the rapid and sensitive determination of multi-species type I interferon. PLoS One 6:e25858. https://doi.org/10.1371/journal.pone.0025858.
38. Motulsky HJ, Brown RE. 2006. Detecting outliers when fitting data with nonlinear regression–a new method based on robust nonlinear regression and the false discovery rate. BMC Bioinformatics 7:123. https://doi.org/10.1186/1471-2105-7-123.
39. Carrillo B, Choi JM, Bornholdt ZA, Sankaran B, Rice AP, Prasad BV. 2014. The influenza A virus protein NS1 displays structural polymorphism. J Virol 88:4113–4122. https://doi.org/10.1128/JVI.03692-13.
40. Chin AW, Li OT, Mok CK, Ng MK, Peiris M, Poon LL. 2014. Influenza A viruses with different amino acid residues at PB2-627 display distinct replication properties in vitro and in vivo: revealing the sequence plasticity of PB2-627 position. Virology 468–470:545–555. https://doi.org/10.1016/j.virol.2014.09.008.
41. Pflug A, Gaudon S, Resa-Infante P, Lethier M, Reich S, Schulze WM, Cusack S. 2018. Capped RNA primer binding to influenza polymerase and implications for the mechanism of cap-binding inhibitors. Nucleic Acids Res 46:956–971. https://doi.org/10.1093/nar/gkx1210.
42. Zhang Y, Aevermann BD, Anderson TK, Burke DF, Dauphin G, Gu Z, He S, Kumar S, Larsen CN, Lee AJ, Li X, Macken C, Mahaffey C, Pickett BE, Reardon B, Smith T, Stewart L, Suloway C, Sun G, Tong L, Vincent AL, Walters B, Zaremba S, Zhao H, Zhou L, Zmasek C, Klem EB, Scheuermann RH. 2017. Influenza Research Database: an integrated bioinformatics resource for influenza virus research. Nucleic Acids Res 45:D466–D474. https://doi.org/10.1093/nar/gkw857.
43. Guan Y, Peiris J, Lipatov A, Ellis T, Dyrting K, Krauss S, Zhang L, Webster R, Shortridge K. 2002. Emergence of multiple genotypes of H5N1 avian influenza viruses in Hong Kong SAR. Proc Natl Acad Sci U S A 99:8950–8955. https://doi.org/10.1073/pnas.132268999.
44. Liedmann S, Hrincius ER, Guy C, Anhlan D, Dierkes R, Carter R, Wu G, Staeheli P, Green DR, Wolff T, McCullers JA, Ludwig S, Ehrhardt C. 2014. Viral suppressors of the RIG-I-mediated interferon response are pre-packaged in influenza virions. Nat Commun 5:5645. https://doi.org/10.1038/ncomms6645.
45. Frensing T, Kupke SY, Bachmann M, Fritzsche S, Gallo-Ramirez LE, Reichl U. 2016. Influenza virus intracellular replication dynamics, release kinetics, and particle morphology during propagation in MDCK cells. Appl Microbiol Biotechnol 100:7181–7192. https://doi.org/10.1007/s00253-016-7542-4.
46. Schneider-Poetsch T, Ju J, Eyler DE, Dang Y, Bhat S, Merrick WC, Green R, Shen B, Liu JO. 2010. Inhibition of eukaryotic translation elongation by cycloheximide and lactimidomycin. Nat Chem Biol 6:209–217. https://doi.org/10.1038/nchembio.304.
47. Marcus PI, Rodriguez LL, Sekellick MJ. 1998. Interferon induction as a quasispecies marker of vesicular stomatitis virus populations. J Virol 72:542–549. https://doi.org/10.1128/JVI.72.1.542-549.1998.
48. Aydillo T, Ayllon J, Pavlisin A, Martinez-Romero C, Tripathi S, Mena I, Moreira-Soto A, Vicente-Santos A, Corrales-Aguilar E, Schwemmle M, Garcia-Sastre A. 2018. Specific mutations in the PB2 protein of influenza A virus compensate for the lack of efficient interferon antagonism of the NS1 protein of bat influenza A-like viruses. J Virol 92:e02021-17. https://doi.org/10.1128/JVI.02021-17.
49. Garcia-Sastre A. 2011. Induction and evasion of type I interferon responses by influenza viruses. Virus Res 162:12–18. https://doi.org/10.1016/j.virusres.2011.10.017.
50. Aragón T, de la Luna S, Novoa I, Carrasco L, Ortín J, Nieto A. 2000. Eukaryotic translation initiation factor 4GI is a cellular target for NS1 protein, a translational activator of influenza virus. Mol Cell Biol 20:6259–6268. https://doi.org/10.1128/mcb.20.17.6259-6268.2000.
51. Hutchinson EC, Charles PD, Hester SS, Thomas B, Trudgian D, Martinez-Alonso M, Fodor E. 2014. Conserved and host-specific features of influenza virion architecture. Nat Commun 5:4816. https://doi.org/10.1038/ncomms5816.
52. Wandzik JM, Kouba T, Karuppasamy M, Pflug A, Drncova P, Provaznik J, Azevedo N, Cusack S. 2020. A structure-based model for the complete transcription cycle of influenza polymerase. Cell 181:877–893. https://doi.org/10.1016/j.cell.2020.03.061.
53. Thierry E, Guilligay D, Kosinski J, Bock T, Gaudon S, Round A, Pflug A, Hengrung N, El Omari K, Baudin F, Hart DJ, Beck M, Cusack S. 2016. Influenza polymerase can adopt an alternative configuration involving a radical repacking of PB2 domains. Mol Cell 61:125–137. https://doi.org/10.1016/j.molcel.2015.11.016.

54. Yamaji R, Yamada S, Le MQ, Li C, Chen H, Qurnianingsih E, Nidom CA, Ito M, Sakai-Tagawa Y, Kawaoka Y. 2015. Identification of PB2 mutations responsible for the efficient replication of H5N1 influenza viruses in human lung epithelial cells. J Virol 89:3947–3956. https://doi.org/10.1128/JVI.03328-14.
55. Pica N, Langlois RA, Krammer F, Margine I, Palese P. 2012. NS1-truncated live attenuated virus vaccine provides robust protection to aged mice from viral challenge. J Virol 86:10293–10301. https://doi.org/10.1128/JVI.01131-12.
56. Beyer WE, Palache AM, de Jong JC, Osterhaus AD. 2002. Cold-adapted live influenza vaccine versus inactivated vaccine: systemic vaccine reactions, local and systemic antibody response, and vaccine efficacy: a meta-analysis. Vaccine 20:1340–1353. https://doi.org/10.1016/s0264-410x(01)00471-6.
57. Gorse GJ, Campbell MJ, Otto EE, Powers DC, Chambers GW, Newman FK. 1995. Increased anti-influenza A virus cytotoxic T cell activity following vaccination of the chronically Ill elderly with live attenuated or inactivated influenza virus vaccine. J Infect Dis 172:1–10. https://doi.org/10.1093/infdis/172.1.1.
58. Brandtzaeg P. 2003. Role of mucosal immunity in influenza. Dev Biol (Basel) 115:39–48.
59. Nguyen HH, Moldoveanu Z, Novak MJ, Van Ginkel FW, Ban E, Kiyono H, McGhee JR, Mestecky J. 1999. Heterosubtypic immunity to lethal influenza A virus infection is associated with virus-specific CD8$^+$ cytotoxic T lymphocyte responses induced in mucosa-associated tissues. Virology 254:50–60. https://doi.org/10.1006/viro.1998.9521.
60. Tumpey TM, Renshaw M, Clements JD, Katz JM. 2001. Mucosal delivery of inactivated influenza vaccine induces B-cell-dependent heterosubtypic cross-protection against lethal influenza A H5N1 virus infection. J Virol 75:5141–5150. https://doi.org/10.1128/JVI.75.11.5141-5150.2001.
61. Mueller SN, Langley WA, Carnero E, García-Sastre A, Ahmed R. 2010. Immunization with live attenuated influenza viruses that express altered NS1 proteins results in potent and protective memory CD8$^+$ T-cell responses. J Virol 84:1847–1855. https://doi.org/10.1128/JVI.01317-09.
62. Fernandez-Sesma A, Marukian S, Ebersole BJ, Kaminski D, Park MS, Yuen T, Sealfon SC, Garcia-Sastre A, Moran TM. 2006. Influenza virus evades innate and adaptive immunity via the NS1 protein. J Virol 80:6295–6304. https://doi.org/10.1128/JVI.02381-05.
63. Jegaskanda S, Vanderven HA, Tan HX, Alcantara S, Wragg KM, Parsons MS, Chung AW, Juno JA, Kent SJ. 2018. Influenza virus infection enhances antibody-mediated NK cell functions via type I interferon-dependent pathways. J Virol 93:e02090-18. https://doi.org/10.1128/JVI.02090-18.
64. Ye L, Schnepf D, Becker J, Ebert K, Tanriver Y, Bernasconi V, Gad HH, Hartmann R, Lycke N, Staeheli P. 2019. Interferon-lambda enhances adaptive mucosal immunity by boosting release of thymic stromal lymphopoietin. Nat Immunol 20:593–601. https://doi.org/10.1038/s41590-019-0345-x.
65. Karpala AJ, Bingham J, Schat KA, Chen L-M, Donis RO, Lowenthal JW, Bean AG. 2011. Highly pathogenic (H5N1) avian influenza induces an inflammatory T helper type 1 cytokine response in the chicken. J Interferon Cytokine Res 31:393–400. https://doi.org/10.1089/jir.2010.0069.
66. Swayne DE. 2007. Understanding the complex pathobiology of high pathogenicity avian influenza viruses in birds. Avian Dis 51:242–249. https://doi.org/10.1637/7763-110706-REGR.1.
67. Suzuki K, Okada H, Itoh T, Tada T, Mase M, Nakamura K, Kubo M, Tsukamoto K. 2009. Association of increased pathogenicity of Asian H5N1 highly pathogenic avian influenza viruses in chickens with highly efficient viral replication accompanied by early destruction of innate immune responses. J Virol 83:7475–7486. https://doi.org/10.1128/JVI.01434-08.
68. Penski N, Härtle S, Rubbenstroth D, Krohmann C, Ruggli N, Schusser B, Pfann M, Reuter A, Gohrbandt S, Hundt J, Veits J, Breithaupt A, Kochs G, Stech J, Summerfield A, Vahlenkamp T, Kaspers B, Staeheli P. 2011. Highly pathogenic avian influenza viruses do not inhibit interferon synthesis in infected chickens but can override the interferon-induced antiviral state. J Virol 85:7730–7741. https://doi.org/10.1128/JVI.00063-11.
69. Du Y, Xin L, Shi Y, Zhang TH, Wu NC, Dai L, Gong D, Brar G, Shu S, Luo J, Reiley W, Tseng YW, Bai H, Wu TT, Wang J, Shu Y, Sun R. 2018. Genome-wide identification of interferon-sensitive mutations enables influenza vaccine design. Science 359:290–296. https://doi.org/10.1126/science.aan8806.
70. Wu NC, Young AP, Al-Mawsawi LQ, Olson CA, Feng J, Qi H, Luan HH, Li X, Wu TT, Sun R. 2014. High-throughput identification of loss-of-function mutations for anti-interferon activity in the influenza A virus NS segment. J Virol 88:10157–10164. https://doi.org/10.1128/JVI.01494-14.
71. Russell AB, Elshina E, Kowalsky JR, Te Velthuis AJ, Bloom JD. 2019. Single-cell virus sequencing of influenza infections that trigger innate immunity. J Virol 93:e00500-19. https://doi.org/10.1128/JVI.00500-19.
72. Russell AB, Trapnell C, Bloom JD. 2018. Extreme heterogeneity of influenza virus infection in single cells. Elife 7:e32303. https://doi.org/10.7554/eLife.32303.
73. Killip MJ, Jackson D, Perez-Cidoncha M, Fodor E, Randall RE. 2017. Single-cell studies of IFN-beta promoter activation by wild-type and NS1-defective influenza A viruses. J Gen Virol 98:357–363. https://doi.org/10.1099/jgv.0.000687.
74. Schat K, Sellers H. 2008. Cell-culture methods, p 195–203. *In* Dufour-Zavala L (ed), A laboratory manual for the identification and characterization of avian pathogens, 5th ed. American Association of Avian Pathologists, Jacksonville, FL.
75. Carver DH, Marcus PI. 1967. Enhanced interferon production from chick embryo cells aged in in vitro. Virology 32:247–257. https://doi.org/10.1016/0042-6822(67)90274-7.
76. Li J, Rahmeh A, Brusic V, Whelan SP. 2009. Opposing effects of inhibiting cap addition and cap methylation on polyadenylation during vesicular stomatitis virus mRNA synthesis. J Virol 83:1930–1940. https://doi.org/10.1128/JVI.02162-08.
77. Alnaji FG, Holmes JR, Rendon G, Vera JC, Fields CJ, Martin BE, Brooke CB. 2019. Sequencing framework for the sensitive detection and precise mapping of defective interfering particle-associated deletions across influenza A and B viruses. J Virol 93:e00354-19. https://doi.org/10.1128/JVI.00354-19.
78. Borges V, Pinheiro M, Pechirra P, Guiomar R, Gomes JP. 2018. INSaFLU: an automated open web-based bioinformatics suite "from-reads" for influenza whole-genome-sequencing-based surveillance. Genome Med 10:46. https://doi.org/10.1186/s13073-018-0555-0.
79. Shepard SS, Meno S, Bahl J, Wilson MM, Barnes J, Neuhaus E. 2016. Viral deep sequencing needs an adaptive approach: IRMA, the iterative refinement meta-assembler. BMC Genomics 17:708. https://doi.org/10.1186/s12864-016-3030-6.
80. Lee C-W. 2014. Reverse genetics of influenza virus, p 37–50. *In* Spackman E (ed), Animal influenza virus. Springer, New York, NY.
81. Neumann G, Watanabe T, Ito H, Watanabe S, Goto H, Gao P, Hughes M, Perez DR, Donis R, Hoffmann E, Hobom G, Kawaoka Y. 1999. Generation of influenza A viruses entirely from cloned cDNAs. Proc Natl Acad Sci U S A 96:9345–9350. https://doi.org/10.1073/pnas.96.16.9345.
82. Zheng L, Baumann U, Reymond JL. 2004. An efficient one-step site-directed and site-saturation mutagenesis protocol. Nucleic Acids Res 32:e115. https://doi.org/10.1093/nar/gnh110.
83. Lee CW, Suarez DL. 2004. Application of real-time RT-PCR for the quantitation and competitive replication study of H5 and H7 subtype avian influenza virus. J Virol Methods 119:151–158. https://doi.org/10.1016/j.jviromet.2004.03.014.
84. Livak KJ, Schmittgen TD. 2001. Analysis of relative gene expression data using real-time quantitative PCR and the $2^{-\Delta\Delta CT}$ method. Methods 25:402–408. https://doi.org/10.1006/meth.2001.1262.
85. Karpala AJ, Lowenthal JW, Bean AG. 2008. Activation of the TLR3 pathway regulates IFN$\beta$ production in chickens. Dev Comp Immunol 32:435–444. https://doi.org/10.1016/j.dci.2007.08.004.
86. Adams SC, Xing Z, Li J, Cardona CJ. 2009. Immune-related gene expression in response to H11N9 low pathogenic avian influenza virus infection in chicken and Pekin duck peripheral blood mononuclear cells. Mol Immunol 46:1744–1749. https://doi.org/10.1016/j.molimm.2009.01.025.
87. Zhang Z, Zou T, Hu X, Jin H. 2015. Type III interferon gene expression in response to influenza virus infection in chicken and duck embryonic fibroblasts. Mol Immunol 68:657–662. https://doi.org/10.1016/j.molimm.2015.10.013.
88. Sarmento L, Afonso CL, Estevez C, Wasilenko J, Pantin-Jackwood M. 2008. Differential host gene expression in cells infected with highly pathogenic H5N1 avian influenza viruses. Vet Immunol Immunopathol 125:291–302. https://doi.org/10.1016/j.vetimm.2008.05.021.
89. Li YP, Handberg KJ, Juul-Madsen HR, Zhang MF, Jorgensen PH. 2007. Transcriptional profiles of chicken embryo cell cultures following infection with infectious bursal disease virus. Arch Virol 152:463–478. https://doi.org/10.1007/s00705-006-0878-9.
90. Cheng Y, Sun Y, Wang H, Yan Y, Ding C, Sun J. 2015. Chicken STING mediates activation of the IFN gene independently of the RIG-I gene. J Immunol 195:3922–3936. https://doi.org/10.4049/jimmunol.1500638.